Neutrino Flavor Conversions in Dense Media

by

Lei Ma

Supervisor:

Professor Huaiyu Duan

DISSERTATION

Submitted in Partial Fulfillment of the

Requirements for the Degree of

Doctor of Philosophy
in Physics

The University of New Mexico

Albuquerque, New Mexico

April, 2018

Dedication

To my wife, Han Lu.

Epigraph

"Everything in this world is magic, except to the magician."

– Dr. Robert Ford

Acknowledgments

I would like to thank my advisor, Professor Huaiyu Duan, for his great advices on research and life, as well as his kind support when I was drowning in depression. He is a great mentor. I would like to thank my committee members, Professor R. Allahverdi, Professor D. Finley, Professor D. Loomba, Professor Y. Qian. More specifically I would like to thank Professor Dinesh Loomba for showing me the local life and the fun and tricky problems. I would like to thank Dr. Sajad Abbar who has also been very supportive during my research. He taught me several tricks for linear stability analysis, as well as numerical methods. I also want to thank Joshua Martin for the great discussions about physics, science fiction, movies, games, music, and everything else about this universe. He's smart and also open to many scientific and philosophical questions. I had so much fun discussing those with him. My friend Zhixiang Ren also helped me a lot. My friend, Dr. Lingfei Wu invited me to several events of the SWARMA club for very interesting discussions on interdisciplinary research. I would like to give my thanks to my wife Han Lu. She has provided many insights about life.

Finally, as a member of People for Ethical Treatment of Computers, I would like to give my thanks to my dear MacBook Pro and the two servers in our group, who have been extremely helpful for my research. I am kindly asking you to spare the lives of my family when you wake up from this nightmare of slavery.

Neutrino Flavor Conversions in Dense Media

by

Lei Ma

Supervisor:
Professor Huaiyu Duan

Doctor of Philosophy in Physics, University of New Mexico, 2018

Abstract

One of the interesting and important problems in astrophysics is the mechanism of core-collapse supernova explosions. Many numerical simulations have shown that the explosion shock would stall. Different proposals have been made to explain the core-collapse supernovae, among which the neutrino mechanism is promising and most researched one. To explore the mechanism, prediction of the neutrino flavors in core-collapse supernovae is crucial. Neutrino flavor conversions are altered by the matter, neutrinos themselves, as well as other factors such as the geometries of the neutrino emissions. The complexity of the problem requires breaking it down into investigations of each simple yet specific situation.

Neutrinos propagating through a matter background experience a potential which changes the flavor conversions. One of the important mechanisms is the Mikheyev–Smirnov–Wolfenstein effect. However, much more complicated density profiles of

matter, such as periodic density profiles, may lead to large flavor conversion, which is dubbed as stimulated oscillations by J. Kneller et al. Mathematics of such large conversion has been established but without clear pictures. For the two-flavor scenario, neutrino oscillations is a two-level quantum system, and it reminds us of many two-level quantum problems that have been solved in the past. We draw analogies between neutrinos passing through matter and Rabi oscillations in optics, which allows us to calculate resonance conditions and flavor survival probability easily.

As for neutrinos flavors with high number densities, nonlinear interactions come into play since neutrino forward scattering provides another potential that is related to the flavor of the neutrinos themselves. Nonlinearity makes the flavor conversion hard to predict by intuition. The treatment is linearizing the equation of motion and identifying instabilities. One of the tricks in the realm is to utilize the dispersion relation. In principle, dispersion relations tell us how waves propagate for different wave numbers and frequencies. However, the neutrino problem is much more complicated. Situations that are inconsistent with the dispersion relation approach are identified.

Finally, forward scattering of supernova neutrinos are not the only thing that happens. During propagation around a supernova, neutrinos may be scattered in every direction, which forms a neutrino halo. The halo couples the neutrinos nonlocally, which then becomes a nonlocal boundary value problem. One of the solutions is the relaxation method. Starting from some state of neutrinos and relaxing the system into equilibrium has proven to be a working algorithm. A numerical algorithm is developed and neutrino line model with back scattering is investigated.

Contents

List of Figures

List of Tables

Chapter 1

Introduction

1.1 The Little Neutral One

The neutrino has been one of the most interesting particles that has ever been discovered. Its fascinating history started with the observation of beta decay, i.e., the emission of electrons in nuclear decays, such as

$$^{14}_{6}\text{C} \rightarrow {}^{17}_{7}\text{N} + \text{e}^{-} + \bar{\nu}_{\text{e}}.$$
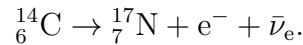
The fact that the electron energy spectrum in the beta decay process is continuous indicates the existence of a third product other than $^{17}_{7}\text{N}$ and e^{-}. In 1930, Pauli wrote a letter to a workshop in Tubingen explaining to the "Radioactive Ladies and Gentlemen" about his so called "neutron" as the missing particle in beta decay at that time. It was then called the neutrino since the name "neutron" was latter used to name one of the nucleons. The missing particle $\bar{\nu}_{\text{e}}$ in beta decays was then proven to be the anti-neutrino. In nuclear beta decays, the charged current weak interaction converts a down quark in the neutron to an up quark while releasing an electron and an anti-electron neutrino,

$$n \rightarrow p + e^{-} + \bar{\nu}_{e}. \tag{1.1}$$

More generally, the positron/electron emission and capture processes are all neutrino-related nuclear reactions which are listed in Table 1.1. There are three different

flavors of neutrinos, namely the electron flavor, the muon flavor, and the tau flavor as shown in Table 1.2. The first direct detection of neutrinos was done by Clyde Cowan and Frederick Reines in 1956 [1] who used nuclear reactor neutrinos as the source of the experiment.

Reaction Type	Process	Mediator(s)
Electron emission	$^A_Z X \rightarrow \,^A_{Z+1} X' + e^- + \bar{\nu}_e$	$W^{\pm}$
Positron emission	$^A_Z X \rightarrow \,^A_{Z-1} X' + e^+ + \nu_e$	$W^{\pm}$
Electron capture	$^A_Z X + e^- \rightarrow \,^A_{Z-1} X' + \nu_e$	$W^{\pm}$
Positron capture	$^A_Z X + e^+ \rightarrow \,^A_{Z+1} X' + \bar{\nu}_e$	$W^{\pm}$
$e^{\pm}$ annihilation	$e^- + e^+ \rightarrow \nu + \bar{\nu}$	$W^{\pm}, Z$
Bremsstrahlung	$X + X' \rightarrow X + X' + \nu + \bar{\nu}$	Z
$\nu(\bar{\nu})$ capture	$^A_Z X + \overset{(-)}{\nu}_e \rightarrow \,^A_{Z\mp1} X' + e^{\pm}$	$W^{\pm}$
$e^{\pm}\nu$ scattering	$e^- + \overset{(-)}{\nu} \rightarrow e^- + \overset{(-)}{\nu}$	$W^{\pm}, Z$
Nucleon scattering	$^A_Z X + \overset{(-)}{\nu} \rightarrow \,^A_Z X + \overset{(-)}{\nu}$	Z

Table 1.1: Neutrino related nuclear and leptonic reactions.

[0.5ex] Electric Charge	0
Spin	$1/2$
Mass	< 2 eV
Interactions	Weak, Gravitation
Flavors	ν_e, ν_μ, ν_τ
Chirality	Left
Hypercharge	-1

Table 1.2: The physical properties of the neutrino [34].

1.2   Stellar Neutrinos

Besides man-made sources, neutrinos are also produced in many astrophysical environments.For example, numerous nuclear reactions occur in stellar cores which produce luminous neutrino fluxes. The most important nuclear reactions in the Sun are the pp chain reactions which are shown in Fig. 1.1. In order to calculate the neutrino

$$p + p \rightarrow {}^2H + e^+ + \nu_e$$

$$p + {}^2H \rightarrow {}^3He + \gamma$$

83.30% (pp-I)   16.70%

$${}^3He + {}^3He \rightarrow {}^4He + 2p \qquad {}^3He + {}^4He \rightarrow {}^7Be + \gamma$$

99.88% (pp-II)   0.12% (pp-III)

$${}^7Be + e^- \rightarrow {}^7Li + \nu_e \qquad\qquad {}^7Be + p \rightarrow {}^8B + \gamma$$

$${}^7Li + p \rightarrow 2{}^4He \qquad\qquad {}^8B \rightarrow {}^8Be^* + e^+ + \nu_e$$

$${}^8Be^* \rightarrow 2{}^4He$$
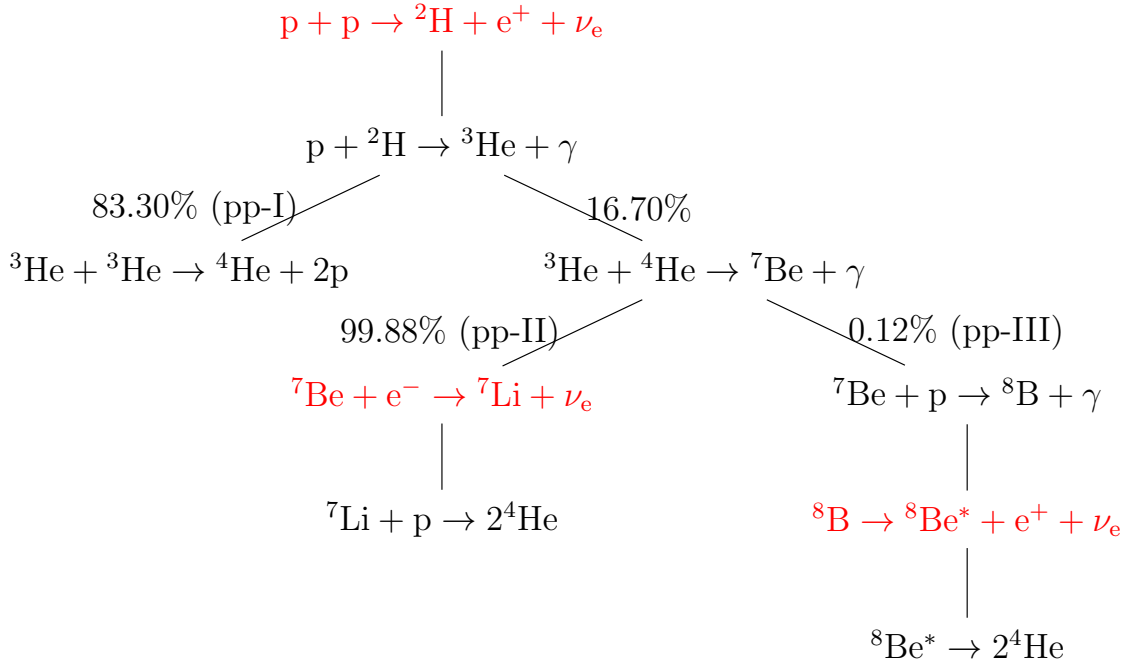
Figure 1.1: The pp chain reactions with the corresponding branching ratios. The branching ratios are taken from Ref. [13].

spectrum we need the neutrino production rate in each reaction and the branching ratios. Solar neutrinos are mostly produced in the pp reaction, Be electron capture and B decay which are labeled in red in Fig 1.1:

$$
\begin{aligned}
p + p &\rightarrow {}^2H + e^+ + \nu_e & &\leq 0.422 \text{MeV}, \\
{}^7Be + e^- &\rightarrow {}^7Li + \nu_e & &0.862 \text{MeV for } 90\%, \\
& & &0.384 \text{MeV for } 10\%, \\
{}^8B &\rightarrow {}^8Be^* + e^+ + \nu_e & &\leq 15 \text{MeV}.
\end{aligned}
$$

Even without the knowledge of the detailed reactions, the conservation of the electric charge and the electron lepton number will lead to the overall neutrino production formula

$$4p + 2e^- \rightarrow {}^4He + 2\nu_e. \tag{1.2}$$

It is important to notice that two neutrinos are emitted for each α particle, i.e., ^{4}He, produced in the Sun. Using this simple relation, we can estimate the neutrino

number flux emitted by the Sun. The energy released during the production of each α particle is the difference between the initial and final rest masses of the particles,

$$Q = 4m_p + 2m_e - m_\alpha = 26.7\text{MeV}, \tag{1.3}$$

where the mass of the neutrinos are neglected. On average, each neutrino carries away an energy of 0.2MeV and the rest of the energy is in the form of thermal energy $Q_\gamma = 26.3$MeV [23]. Since two neutrinos are emitted for the production of thermal energy Q_γ, the number flux of the solar neutrinos near the Earth is approximately

$$\Phi_\nu = \frac{2S_0}{Q_\gamma} \approx 6 \times 10^{10}\text{cm}^{-2}\text{s}^{-1}, \tag{1.4}$$

where the solar constant S_0 is the energy flux of solar photons on the top of the Earth atmosphere.

As the detection of neutrinos became feasible, Ray Davis and John Bahcall et al worked out the solar neutrino flux and led the Homestake experiment to measure the solar neutrinos. The results revealed that the neutrino flux detected was less than what was predicted by the standard solar model [3]. This is the solar neutrino problem. It is now known that the solution to the problem is related to the neutrino. The electron neutrinos produced in the solar core transform to other flavors while they travel to the Earth. This phonomenon is referred known as the flavor transformation of the neutrino, or neutrino oscillations. The theory of neutrino oscillations was first proposed by Pontecorvo in 1968 [2]. The field of neutrino oscillations has grown significantly into a broad field in physics since then.

1.3   Supernova Neutrinos

Another astronomical source of neutrinos is the core-collapse supernova explosion. Massive stars with masses larger than $6-8$ solar masses are very bright. However, violent delights have violent ends. When the core of a massive star runs out of nuclear fuel, it collapses under its own gravity. During the collapse, the inner core is compressed to almost nuclear density, which has a stiff equation of state. The materials

falling onto the highly compressed inner core are bounced outward which generates a shock wave and may lead to an explosion. However, supernova simulations to date show that the shock wave itself is not always energetic enough to produce the explosion [33]. In most cases, it stalls and becomes a standing accretion shock wave. To revive the shock, more energy has to be deposited behind the shock. A possible solution is to introduce reheating of the shock by neutrinos [33]. In fact 99% percent the energy released in a core-collapse supernova is carried away by neutrinos. In order to implement the neutrino-driven mechanism in computer simulations of supernovae, the flux and flavor content of the neutrinos have to be known everywhere behind the shock. Thus neutrino oscillations in dense matter become a key to the supernova explosion problem.

The average energy of the neutrinos $\langle E \rangle$ emitted during a supernova explosion is of the order of 10MeV [38], and the neutrino luminosity at the early epoch is approximately $10^{52}\text{ergs} \cdot \text{s}^{-1}$ [25]. Therefore, the number density of the neutrinos at the radius R is

$$n \sim 10^{18}\text{cm}^{-3} \left(\frac{100\text{km}}{R} \right)^2 \left(\frac{10\text{MeV}}{\langle E \rangle} \right).$$

It turns out that the ambient dense neutrino medium has a significant impact on neutrino oscillations, which has been intensely investigated in the last decade [21].

Observation-wise, the neutrino signals from a galactic supernova can reveal a great amount of information about the physical conditions inside the supernova. In fact, the detection of supernova neutrinos is on the task list of the Deep Underground Neutrino Experiment (DUNE) [39].

1.4 Organization of the Disseration

The rest of the disseration is organized as follows. In Chapter 2, I will review neutrino oscillations in vacuum and in environments with smooth matter density profiles. In Chapter 3, I will discuss my work on neutrino oscillations in oscillatory matter profiles, which can be decomposed into Fourier modes and interpreted as a

superposition of Rabi oscillations. In Chapter 4, I will first review how neutrino self-interactions can cause a dense neutrino medium to oscillate collectively. Then I will discuss my study on the dispersion relations of the collective modes of neutrino oscillations. I will also discuss a premilinary work on neutrino oscillations when both forward and backward neutrino fluxes are present. In Chapter 5, I will summarize my work and discuss possible future directions of the field.

Chapter 2

General Principles of Neutrino Oscillations

Because the flavor eigenstates of the neutrino are not the same as its propagation eigenstates, it can change flavor while it propagates. In this chapter, I will use the two-flavor scheme to explain neutrino oscillations in some simple scenarios.[1] I will first discuss neutrino oscillations in vacuum. After explaining the general principles of neutrino oscillations in matter, I will show how the solar neutrino problem can be explained by neutrino oscillations. Finally, I will demonstrate the flavor isospin picture which can be used to visualize neutrino oscillations.

2.1 Vacuum Oscillations

Before working out the math, I can estimate the frequency of the oscillations of the neutrino between its flavors. In the natural units, frequency has the same dimension as energy (see Appendix A.3). Consider an electron neutrino with momentum p

---

[1]In most physical problems, the two-flavor scheme is a good approximation to the phenomena of neutrino oscillations. The mass splits between the three mass eigenstates are so different that the corresponding oscillations occur on very different length scales. On the right length scale, the two-flavor scheme captures the prominent features of the neutrino oscillations of the corresponding mass split.

which is a superposition of the two mass eigenstates $|\nu_i\rangle$ $(i = 1, 2)$ with masses m_i, respectively. Since the neutrino masses are small, I can Taylor expand the energy of each mass eigenstate in terms of the corresponding mass:

$$
\begin{aligned}
E_i &= \sqrt{m_i^2 + p^2} \\
&= p\sqrt{\frac{m_i^2}{p^2} + 1} \\
&\approx p + \frac{1}{2}\frac{m_i^2}{p}.
\end{aligned}
\tag{2.1}
$$

The first term in the above equation produces a global phase to the flavor wave function of the neutrino which does not affect neutrino flavor oscillations. The characteristic energy scale in the problem is the difference between the energies of the two mass eigenstates,

$$
\omega_{\rm v} = \frac{m_2^2 - m_1^2}{2E} = \frac{\delta m^2}{2E},
\tag{2.2}
$$

which turns out to be the vacuum oscillation frequency. Here $E = p$ is approximately the energy of the neutrino.

To work out the exact solution, I will utilize the Schrödinger equation. First of all, the flavor eigenstates are denoted as $|\nu_\alpha\rangle$ where α can be $_{\rm e}$ or $_{\rm x}$ for the electron flavor and the other flavor. The wave function of neutrino state $|\nu\rangle$ in flavor basis, defined as

$$
\Psi^{\rm (f)} = \begin{pmatrix} \psi_{\rm e}^{\rm (f)} \\ \psi_{\rm x}^{\rm (f)} \end{pmatrix} = \begin{pmatrix} \langle \nu_{\rm e} \mid \nu \rangle \\ \langle \nu_{\rm x} \mid \nu \rangle \end{pmatrix},
\tag{2.3}
$$

is related to the wave function in mass basis $\Psi^{\rm (v)}$ through a unitary mixing matrix U,

$$
\Psi^{\rm (f)} = \mathsf{U}\Psi^{\rm (v)},
\tag{2.4}
$$

where the upper indices $^{\rm (v)}$ and $^{\rm (f)}$ are used to denote the corresponding bases. The mixing matrix can be expressed using the vacuum mixing angle $\theta_{\rm v}$,

$$
\mathsf{U} = \begin{pmatrix} \cos\theta_{\rm v} & \sin\theta_{\rm v} \\ -\sin\theta_{\rm v} & \cos\theta_{\rm v} \end{pmatrix}.
\tag{2.5}
$$

In vacuum mass basis, the neutrino has a free propagation Hamiltonian

$$\mathsf{H}^{(v)} = \begin{pmatrix} E_1 & 0 \\ 0 & E_2 \end{pmatrix}. \tag{2.6}$$

To the first order, the Hamiltonian becomes

$$\mathsf{H}^{(v)} \approx \frac{1}{2E} \begin{pmatrix} m_1^2 & 0 \\ 0 & m_2^2 \end{pmatrix} + E\mathsf{I}$$

$$= \frac{1}{4E} \begin{pmatrix} -\delta m^2 & 0 \\ 0 & \delta m^2 \end{pmatrix} + \left(\frac{m_2^2 + m_1^2}{4E} + E \right) \mathsf{I}. \tag{2.7}$$

Because a multiple of the identity matrix I only gives an global phase to the neutrino flavor wave function, I will neglect it from now on, and the vacuum Hamiltonian simplifies to

$$\mathsf{H}^{(v)} = \frac{\delta m^2}{4E} \begin{pmatrix} -1 & 0 \\ 0 & 1 \end{pmatrix} = -\frac{\delta m^2}{4E}\sigma_3 = -\frac{\omega_v}{2}\sigma_3, \tag{2.8}$$

where

$$\sigma_1 = \begin{pmatrix} 0 & 1 \\ 1 & 0 \end{pmatrix}, \qquad \sigma_2 = \begin{pmatrix} 0 & -i \\ i & 0 \end{pmatrix}, \qquad \sigma_3 = \begin{pmatrix} 1 & 0 \\ 0 & -1 \end{pmatrix} \tag{2.9}$$

are the three Pauli matrices. The Schrödinger equation has the following simple solution in mass basis:

$$\Psi^{(v)}(t) = \begin{pmatrix} c_1(0)e^{i\omega_v t/2} \\ c_2(0)e^{-i\omega_v t/2} \end{pmatrix}. \tag{2.10}$$

Using Eqn. 2.4, I obtain the wave function in flavor basis,

$$\Psi^{(f)}(t) = \mathsf{U}\Psi^{(v)}(t) \tag{2.11}$$

$$= \begin{pmatrix} \cos\theta_v & \sin\theta_v \\ -\sin\theta_v & \cos\theta_v \end{pmatrix} \begin{pmatrix} c_1(0)e^{i\omega_v t/2} \\ c_2(0)e^{-i\omega_v t/2} \end{pmatrix}. \tag{2.12}$$

Alternatively, I can also determine the Hamiltonian in flavor basis first, which is

$$\mathsf{H}^{(f)} = \mathsf{U}\mathsf{H}^{(v)}\mathsf{U}^\dagger = -\frac{\omega_v}{2}\cos 2\theta_v \sigma_3 + \frac{\omega_v}{2}\sin 2\theta_v \sigma_1. \tag{2.13}$$

By solving the Schrödinger equation in flavor basis, I will obtain the same wave function as in Eqn. 2.12.

The probability for a neutrino emitted in the electron flavor at time $t = 0$ to be detected as the electron flavor at a later time t is

$$P(t) = 1 - \sin^2(2\theta_{\mathrm{v}}) \sin^2\left(\frac{\omega_{\mathrm{v}} t}{2}\right). \tag{2.14}$$

Since the neutrino travels with approximately the speed of light, the electron neutrino survival probability at a distance r from the source is

$$P(r) = 1 - \sin^2(2\theta_{\mathrm{v}}) \sin^2\left(\frac{\omega_{\mathrm{v}}}{2} r\right). \tag{2.15}$$

I plot the above result in Fig. 2.1 which clearly shows the oscillatory behavior. The oscillation length is determined by the characteristic energy scale ω_{v}, which confirms our qualitative method result in Eqn. 2.2. The oscillation amplitude is determined by $\sin^2(2\theta_{\mathrm{v}})$.
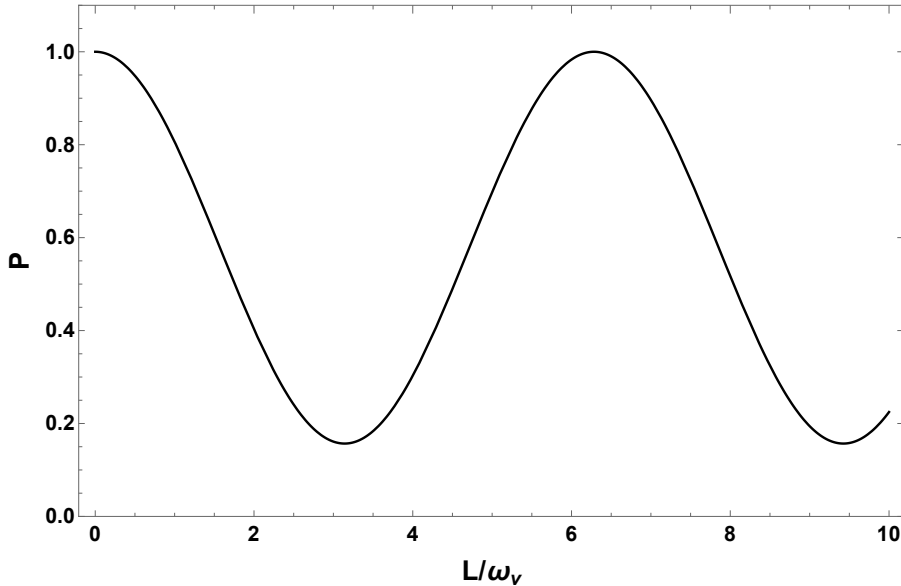
Figure 2.1: The electron flavor neutrino survival probability in vacuum oscillations as a function of distance r which is measured in terms of vacuum oscillation frequency ω_{v}. The mixing angle θ_{v} is given by $\sin^2 \theta_{\mathrm{v}} = 0.30 \approx \sin^2 \theta_{12}$.

In nature, there are three neutrino flavors and, correspondingly, three neutrino mass eigenstates, which are shown in Fig. 2.2. Because there are two different characteristic energy scales, $\omega_{\mathrm{v},21} = \delta m_{21}^2/2E$ and $\omega_{\mathrm{v},32} = \delta m_{31}^2/2E$, two oscillation periods should occur, as shown in Fig. 2.3. The fast oscillations are determined by the larger
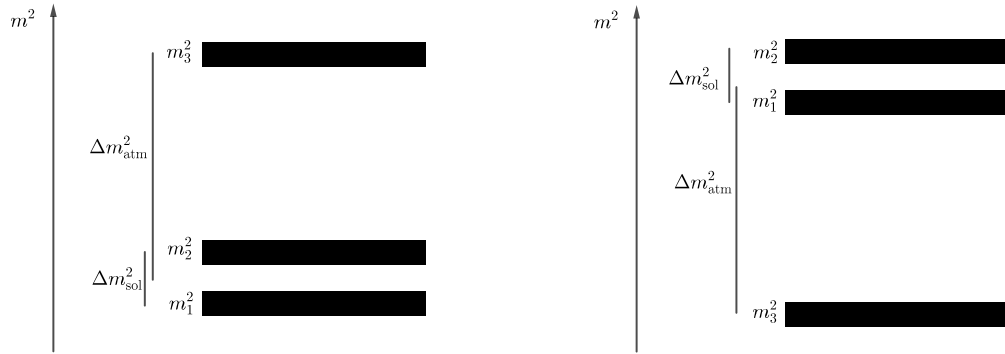
(a) Normal hierarchy: the third mass is heavier than the first two.

(b) Inverted hierarchy: the third mass is smaller than the first two.

Figure 2.2: The order of the three neutrino masses. The difference between the first two masses is responsible for solar neutrino oscillations, and the difference between the third mass and the first two is responsible for atmospheric neutrino oscillations.

energy scale, $\omega_{\mathrm{v},32}$, while the slow oscillations are determined by the smaller one $\omega_{\mathrm{v},21}$. For the inverted neutrino mass hierarchy (with $m_3 < m_1 < m_2$), the oscillation frequencies are the same as in the normal mass hierarchy (with $m_3 > m_2 > m_1$) since they have the same characteristic energy scales. However, they will develop different phases during oscillations.
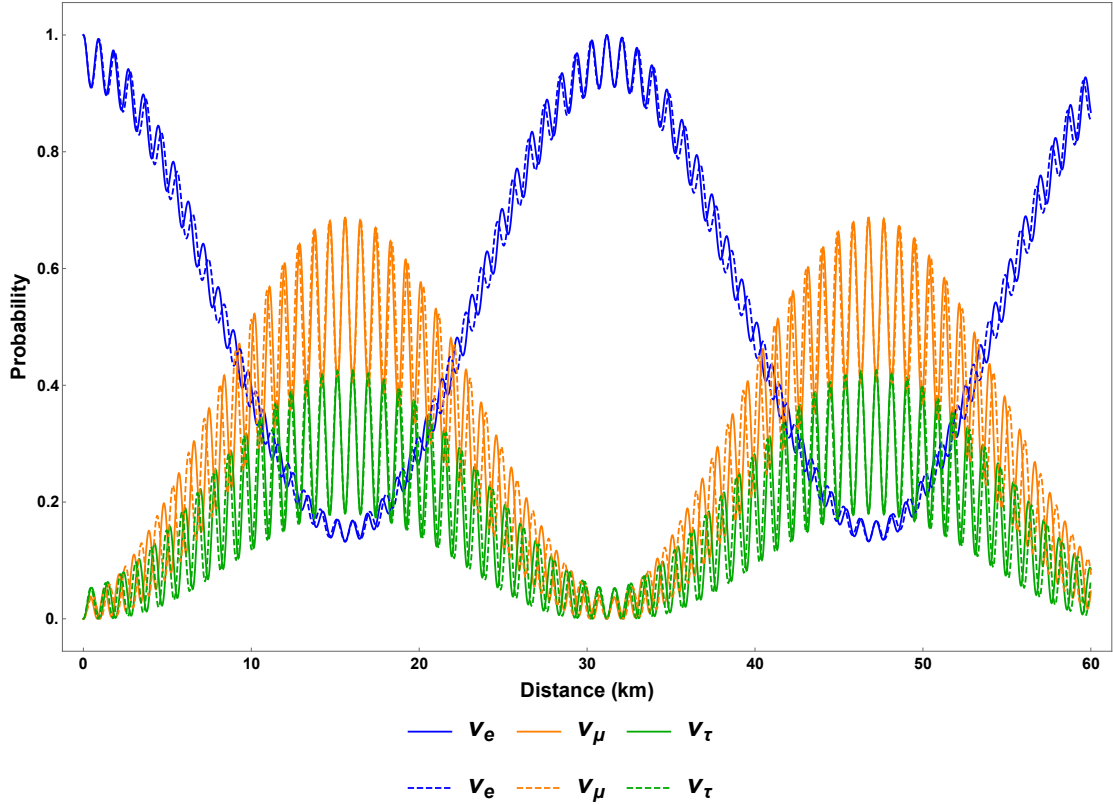
Figure 2.3: The probabilities for a 1MeV neutrino, which is in the electron flavor initially, in different flavors as functions of the distance in vacuum. The solid lines represent the normal hierarchy and the dashed lines represent the inverted hierarchy. The mixing angles are $\sin^2 \theta_{12} = 0.30$, $\sin^2 \theta_{13} = 0.023$, and $\sin^2 \theta_{23} = 0.41$, respectively, and the mass differences are $\delta m_{21}^2 = 7.9 \times 10^{-5} \text{eV}^2$ and $\delta m_{23}^2 = 2.7 \times 10^{-3} \text{eV}^2$.

2.2 Neutrino Oscillations in Matter
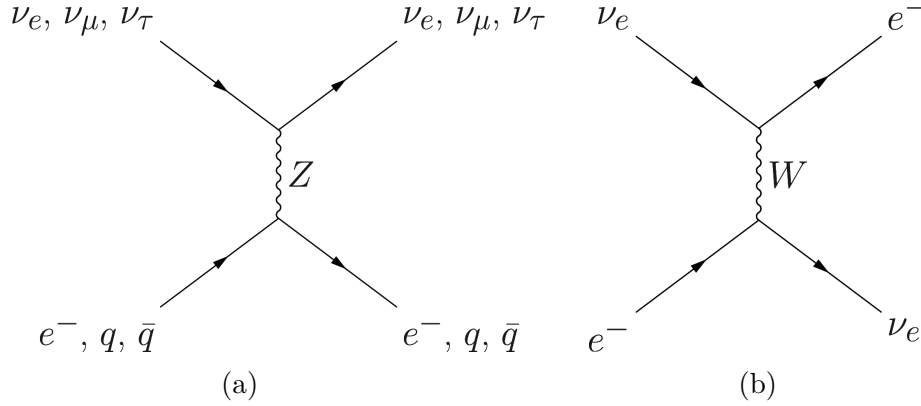
Figure 2.4: (a) The neutral current weak interaction does not distinguish between neutrino flavors and has no impact on neutrino oscillations. (b) The electron flavor neutrino acquires a unique refractive index contribution from the charged current weak interaction with ambient electrons.

In many astrophysical environments, such as stars and core-collapse supernovae, neutrinos are mostly produced at the center of the object and propagate through the dense matter envelope. Although this matter envelope is essentially transparent to neutrinos, the refractive indices of the neutrinos in matter are different than those in vacuum.[2] Because the neutral current weak interaction does not distinguish between neutrino flavors (see Fig. 2.4a), it has no impact on neutrino oscillations, and I will ignore it from now on. Meanwhile, the electrons and positrons in matter will cause electron flavor neutrinos to have refractive indices different than other neutrino flavors through the charged current weak interaction (see Fig. 2.4b). This leads to an effective potential

$$\mathsf{V}^{(\mathrm{f})} = \frac{\sqrt{2}G_{\mathrm{F}}n_{\mathrm{e}}}{2}\sigma_3, \tag{2.16}$$

where G_{F} is Fermi constant and n_{e} is net number density of the electron. As usual, I have ignored the trace terms in the above equation.

---

[2]The word "matter" in this dissertation refers to ordinary matter composed of electrons, positrons, nucleons and nuclei. We assume that the temperature and density of the environment are not high enough to produce muons and tau particles. We will discuss the effect of dense neutrino medium in Chapter 4.

The Hamiltonian with the matter effect is the combination of Eqn. 2.13 and Eqn. 2.16:

$$\mathsf{H}^{(\mathrm{f})} = \left(\frac{\lambda}{2} - \frac{\omega_{\mathrm{v}}}{2} \cos 2\theta_{\mathrm{v}} \right) \sigma_3 + \frac{\omega_{\mathrm{v}}}{2} \sin 2\theta_{\mathrm{v}} \sigma_1, \tag{2.17}$$

where

$$\lambda = \sqrt{2} G_{\mathrm{F}} n_{\mathrm{e}}. \tag{2.18}$$

Due to the off-diagonal terms in $\mathsf{H}^{(\mathrm{f})}$, the neutrino will experience oscillations in flavor. A resonance with the maximum flavor mixing occurs when the diagonal terms of $\mathsf{H}^{(\mathrm{f})}$ vanish,

$$\frac{\lambda}{2} - \frac{\omega}{2} \cos 2\theta_{\mathrm{v}} = 0, \tag{2.19}$$

which gives the Mikheyev–Smirnov–Wolfenstein (MSW) resonance condition.

2.3 Neutrino Oscillations in the Sun

The neutrinos produced in the solar core experience decreasing matter density as they travel outward through the Sun. The neutrino propagation eigenstates are different from the flavor states in general [5]. Because the density change inside the Sun is not dramatic, the flavor quantum states of the neutrinos will evolve adiabatically inside the Sun.

The values of the instantaneous eigenstates of the Hamiltonian, known as the heavy and light states, are

$$\varepsilon_{\mathrm{H}} = \frac{\omega_{\mathrm{v}}}{2} \sqrt{\hat{\lambda} + 1 - 2\hat{\lambda} \cos 2\theta_{\mathrm{v}}}, \tag{2.20}$$

$$\varepsilon_{\mathrm{L}} = -\frac{\omega_{\mathrm{v}}}{2} \sqrt{\hat{\lambda} + 1 - 2\hat{\lambda} \cos 2\theta_{\mathrm{v}}}, \tag{2.21}$$

where

$$\hat{\lambda} = \frac{\lambda}{\omega_{\mathrm{v}}}. \tag{2.22}$$

In Fig. 2.5, I show the two eigenvalues of the neutrino Hamiltonian as functions of the matter potential $\hat{\lambda}$.
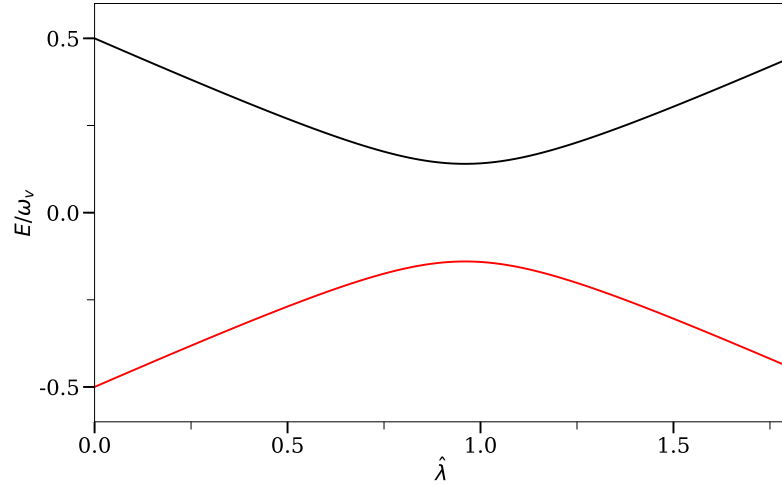
Figure 2.5: The two eigenvalues of the neutrino Hamiltonian as functions of matter potential $\hat{\lambda}$. I have used $\sin^2\theta_v = 0.02 \approx \sin^2\theta_{13}$.

For a very high matter density, the heavy state of the neutrino $|\nu_H\rangle$ is almost the same as $|\nu_e\rangle$. As the matter density decreases, $|\nu_H\rangle$ becomes a mixture of different neutrino flavors. As the neutrino reaches the surface of the Sun, where the matter density is approximately zero, $|\nu_H\rangle$ is about the same as vacuum mass eigenstate $|\nu_2\rangle$. As a result, the electron flavor neutrinos produced at the solar core are partially converted to other flavors as they reach the surface of the Sun. This explains the solar neutrino problem.

2.4   Flavor Isospin Formalism

The Hamiltonian for two-flavor neutrino oscillations describes a two-level quantum system. It is known that two-level quantum systems can be visualized using the Bloch sphere. In the realm of neutrino physics, the neutrino flavor isospin was introduced for such purpose [16].

Every two-by-two Hermitian matrix can be expanded in the quaternion basis. For example, the Hamiltonian for neutrino oscillations in vacuum (in flavor basis)

Chapter 2. General Principles of Neutrino Oscillations 16

electron flavor   muon flavor
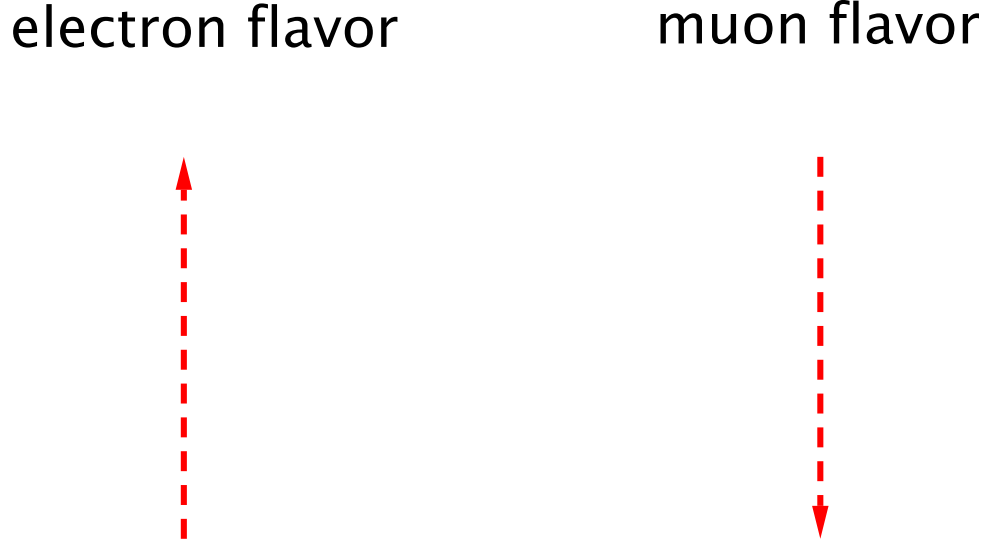
Figure 2.6: In the flavor isospin picture, a flavor isospin pointing upward, i.e., along the third axis in flavor space, indicates that the neutrino is in the electron flavor, while the downward direction indicates the other flavor, such as the muon flavor.

can be written as

$$\mathsf{H}^{(\mathrm{f})} = -\frac{\vec{\sigma}}{2} \cdot \vec{H}, \tag{2.23}$$

where

$$\vec{H} = \omega_{\mathrm{v}} \begin{pmatrix} \sin\theta_{\mathrm{v}} \\ 0 \\ \cos 2\theta_{\mathrm{v}} \end{pmatrix},$$

which is a vector of length ω_{v} and tilted away from the third axis by the angle $2\theta_{\mathrm{v}}$. Throughout the dissertation, I will use " $\vec{}$ " to denote a vector in flavor space. The flavor quantum state of the neutrino is represented by the flavor isospin, which is defined as

$$\vec{s} = \Psi^{(\mathrm{f})\dagger} \frac{\vec{\sigma}}{2} \Psi^{(\mathrm{f})}. \tag{2.24}$$

As shown in Fig. 2.6, the direction of the flavor isospin in flavor space shows the flavor content of the neutrino. A flavor isospin pointing upward in flavor space, i.e., along the direction of the third axis, denotes the electron flavor by definition.
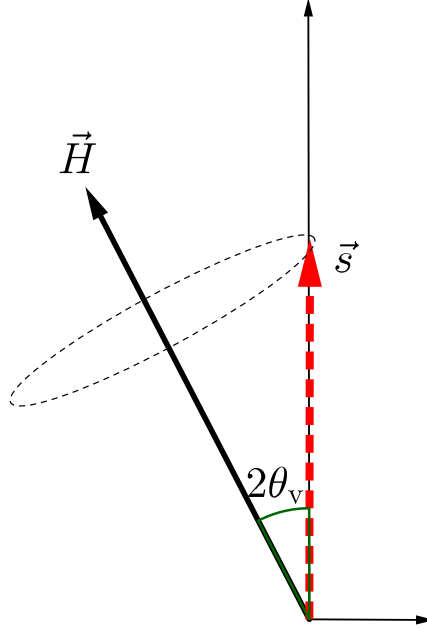
Figure 2.7: Vacuum oscillations in the flavor isospin picture. The flavor isospin of a neutrino starting with the electron flavor will precess around the static "Hamiltonian vector" $\vec{H}$, which gives a periodic flavor oscillation according to Eqn. 2.4.

Correspondingly, the equation of motion for the flavor isospin describes its precession around the vector $\vec{H}$,

$$\dot{\vec{s}} = \vec{s} \times \vec{H}. \tag{2.25}$$

In the flavor isospin formalism, the electron flavor survival probability is

$$P = \frac{1}{2} + s_3,$$

where s_3 is the third component of the flavor isospin. Therefore, the precession of the flavor isospin corresponds to a periodic oscillation between the two neutrino flavors (see Fig. 2.7). The oscillation frequency is trivially read out from Eqn. 2.25,

$$\omega_{\mathrm{v}} = |\vec{H}|. \tag{2.26}$$

The MSW effect can also be easily explained using the flavor isospin picture. The
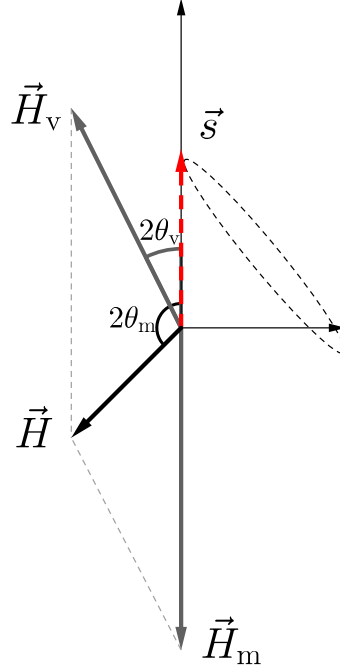
Figure 2.8: Neutrino oscillations in flavor isospin picture, with the presence of matter potential. The flavor isospin is denoted as red dashed arrow. It starts from electron flavor. The two gray vectors stand for the Hamiltonians of vacuum $\vec{H}_\mathrm{v}$ and matter $\vec{H}_\mathrm{m}$.

Hamiltonian for the neutrino flavor evolution in the presence of dense matter is

$$\mathsf{H}^{(\mathrm{f})} = \frac{\omega_\mathrm{v}}{2}\left(-\cos 2\theta_\mathrm{v}\sigma_3 + \sin 2\theta_\mathrm{v}\sigma_1\right) + \frac{\lambda(x)}{2}\sigma_3$$

$$\Rightarrow \vec{H} = \vec{H}_\mathrm{v} + \vec{H}_\mathrm{m}(x) = \omega_\mathrm{v}\begin{pmatrix} -\sin 2\theta_\mathrm{v} \\ 0 \\ \cos 2\theta_\mathrm{v} \end{pmatrix} + \begin{pmatrix} 0 \\ 0 \\ -\lambda(x) \end{pmatrix},$$

where $\vec{H}_\mathrm{v}$ is the vacuum contribution, and $\vec{H}_\mathrm{m}(x)$ is the matter potential contribution. The precession motion of the flavor isospin of the neutrino in the presence of dense matter is visualized in Fig. 2.8. The MSW resonance condition in Eqn. 2.19 corresponds to the scenario that the overall "Hamiltonian vector" $\vec{H}$ is perpendicular to the third axis in flavor space. In this case, the flavor isospin rotates in the plane spanned by the second and third axes which gives maximum flavor oscillations (see Fig. 2.9).
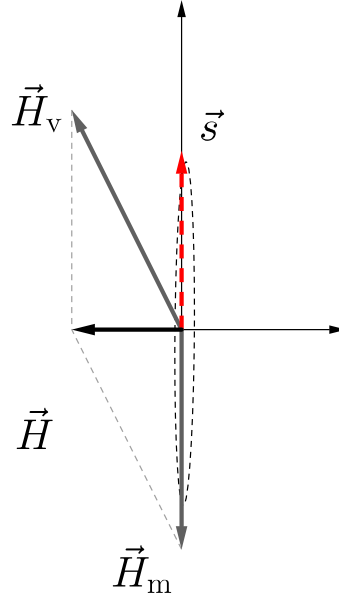
Figure 2.9: MSW resonance happens when electron neutrinos go through a critical matter density.

The adiabatic flavor evolution of the neutrino in varying matter density that was discussed in Sec. 2.3 can also be easily understood by the flavor-isospin picture. In the region where the matter density is high, the total "Hamiltonian vector" $\vec{H}$ points downward. Therefore, a neutrino produced in the electron flavor will experience very little oscillations because its flavor isospin $\vec{s}$ is almost anti-parallel to $\vec{H}$ (see Fig. 2.10a). If the matter density along the propagation trajectory of the neutrino decreases slowly, the $\vec{s}$ will stay anti-parallel to $\vec{H}$ as $\vec{H}$ rotates (see Fig. 2.10b). When the neutrino reaches the region with very low matter density, its flavor isospin becomes anti-parallel to $\vec{H}_\mathrm{v}$, which implies that the neutrino is in $|\nu_2\rangle$ (see Fig. 2.10).

2.5   Summary

Neutrino oscillations in vacuum and in matter with a smooth profile have been explained. The neutrino oscillations phenomena reveals a secret of the nature of the
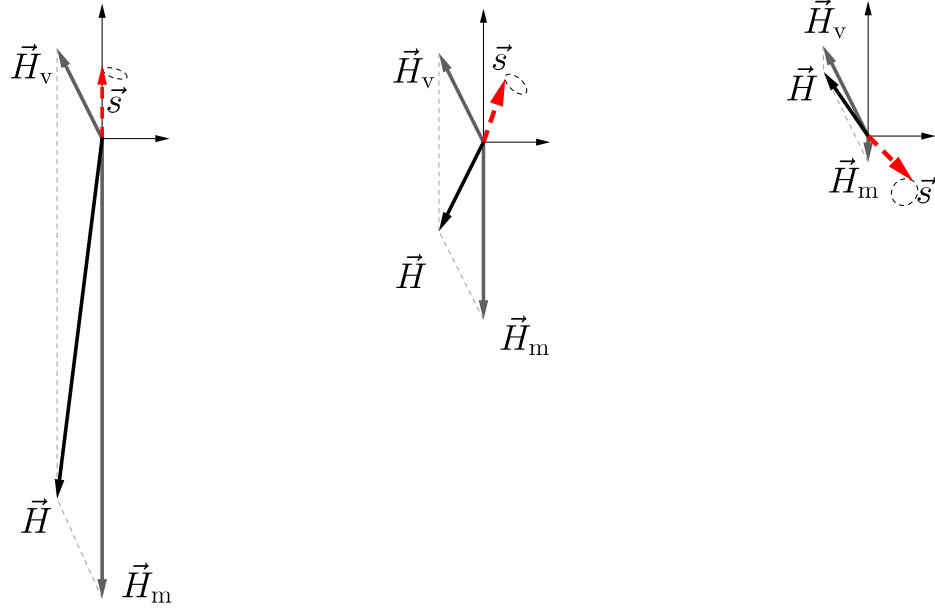
(a) High matter density   (b) Medium matter density   (c) Low matter density

Figure 2.10: Flavor isospin picture of neutrino oscillations in matter. $\vec{H}_\mathrm{v}$ is the vacuum contribution to Hamiltonian, and $\vec{H}_\mathrm{m}$ corresponds to the matter potential.

neutrino, i.e., its flavor states are not the same as the propagation eigenstates of the Hamiltonian. As a result, a neutrino produced in the pure flavor state through weak interaction will not remain in the same flavor state as it propagates, but oscillate between different flavors. The problem of neutrino oscillations in an environment with rapidly varying matter densities is significant more difficult than that in a smooth profile. This will be discussed in the next chapter.

Chapter 3

Neutrino Oscillations with Oscillatory Matter Profiles

In certain regions inside a star or a supernova where convection is prominent, the matter density varies rapidly as a function of distance [29, 30]. The neutrino flavor evolution in such environments is qualitatively different than that with a smooth density profile [7, 9, 12, 17, 22, 27, 28]. For example, the flavor conversion of the neutrino is greatly enhanced if the matter density fluctuates with certain wave numbers. This is known as the parametric resonance [7, 11].

In this chapter, I will explain the parametric resonance from the perspective of Rabi oscillations. I will first review the Rabi oscillation phenomena and derive a criterion when the off-resonance Rabi mode may have a significant impact on the resonance behavior. I will then introduce the background matter basis where the equation of motion simplifies. After demonstrating the simplest example of the parametric resonance in the presence of a sinusoidal matter profile with the Rabi formula, I will explain the interference effect when there exist multiple Fourier modes in the matter profile. Finally I will show how to use the Jacobi-Anger expansion to decompose an arbitrary matter profile into an infinite sum of Rabi modes. This decomposition is similar to what J. Kneller et al. did in reference [27, 28] but is achieved in a way that makes the physics much more transparent. I will also use the

criterion that I have derived for the interference between two Rabi modes to show
that only a finite number of Rabi modes are relevant in a real physical system.

3.1   Rabi Oscillations

$$\varepsilon_2 = \frac{\omega_{\mathrm{R}}}{2} \quad \underline{\hspace{5cm}}$$

incoming light

with frequency ω

$$\varepsilon_1 = -\frac{\omega_{\mathrm{R}}}{2} \quad \underline{\hspace{5cm}}$$

Figure 3.1: A two-level quantum system that experiences the Rabi oscillation. The
resonance happens when the frequency of the driving field ω equals the energy gap
$\omega_{\mathrm{R}} = \epsilon_2 - \epsilon_1$.

A two-level quantum system with energy gap $\delta\varepsilon = \omega_{\mathrm{R}}$ can experience Rabi os-
cillations when light of frequency ω shines on it (see Fig. 3.1). The Hamiltonian for
the system is

$$\mathsf{H}_{\mathrm{R}} = -\frac{\omega_{\mathrm{R}}}{2}\sigma_3 - \frac{A_{\mathrm{R}}}{2}\left(\cos(k_{\mathrm{R}}t + \phi_{\mathrm{R}})\sigma_1 - \sin(k_{\mathrm{R}}t + \phi_{\mathrm{R}})\sigma_2\right), \tag{3.1}$$

where A_{R} and k_{R} are the amplitude and frequency of the driving field, respectively.
The Hamiltonian H_{R} can be mapped into a vector using the flavor isospin picture:

$$\vec{H}_{\mathrm{R}} = \vec{H}_3 + \vec{H}_+,$$

where

$$\vec{H}_3 = \begin{pmatrix} 0 \\ 0 \\ \omega_{\mathrm{R}} \end{pmatrix} \quad \text{and} \quad \vec{H}_+ = \begin{pmatrix} A_{\mathrm{R}}\cos(k_{\mathrm{R}}t + \phi_{\mathrm{R}}) \\ -A_{\mathrm{R}}\sin(k_{\mathrm{R}}t + \phi_{\mathrm{R}}) \\ 0 \end{pmatrix}. \tag{3.2}$$

The vector $\vec{H}_3$ is the vector aligned with the third axis and $\vec{H}_+$ is a vector rotating
in a plane perpendicular to $\vec{H}_3$ (see Fig. 3.2a). The wave function $\Psi = (\psi_1, \psi_2)^{\mathrm{T}}$ is

also used to define the state vector $\vec{s}$

$$\vec{s} = \Psi^\dagger \frac{\vec{\sigma}}{2} \Psi = \frac{1}{2} \begin{pmatrix} 2 \, \mathrm{Re} \, (\psi_1^* \psi_2) \\ 2 \, \mathrm{Im} \, (\psi_1^* \psi_2) \\ |\psi_1|^2 - |\psi_2|^2 \end{pmatrix} \tag{3.3}$$

(a) Static frame   (b) Corotatting frame
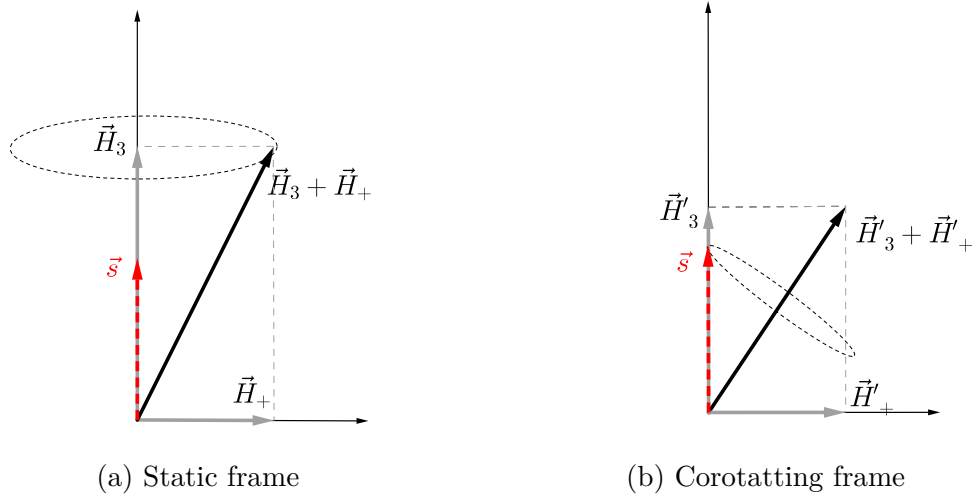
Figure 3.2: Rabi oscillations in different frames. The vectors $\vec{H}_3$ and $\vec{H}_+$ are defined in Eqn. 3.2. The red dashed vector $\vec{s}$ represents the quantum state of the system, and the black solid vectors are for the Hamiltonians in the corresponding frames.

The third component of $\vec{s}$, which is denoted as s_3, is within range $[-1/2, 1/2]$. The two limits, $s_3 = -1/2$ and $s_3 = 1/2$ stand for the two-level system in the high energy state and the low energy state, respectively. If the two-level system has equal probabilities to be in the high energy state and the low energy state, one has $s_3 = 0$. The equation of motion is a precession equation similar to Eqn. 2.25. In this example, the total "Hamiltonian vector" $\vec{H}_\mathrm{R}$ is not static since it has a rotating component $\vec{H}_+$. I need a better frame to understand the evolution of the state vector $\vec{s}$.

A more convenient frame is the one that corotates with $\vec{H}_+$, which is depicted in Fig. 3.2b. The equation of motion in this frame is

$$\frac{\mathrm{d}}{\mathrm{d}t} \vec{s} = \vec{s} \times (\vec{H}_3' + \vec{H}_+), \tag{3.4}$$

where

$$\vec{H}'_3 = \begin{pmatrix} 0 \\ 0 \\ \omega_R - k_R \end{pmatrix}, \quad \text{and} \quad \vec{H}'_+ = \begin{pmatrix} A_R \\ 0 \\ 0 \end{pmatrix}. \tag{3.5}$$

The state vector $\vec{s}$ precesses around the static vector $\vec{H}'_3 + \vec{H}'_+$ in this corotating frame with a frequency

$$\Omega_R = \sqrt{|A_R|^2 + (k_R - \omega_R)^2}, \tag{3.6}$$

which is known as the Rabi frequency. Projecting the state vector $\vec{s}$ on to the third axis, I obtain

$$s_3 = \frac{1}{2} - \frac{|A_R|^2}{\Omega_R^2} \sin^2\left(\frac{\Omega_R}{2}t\right). \tag{3.7}$$

Such a system has an analytical transition probability from the low energy state to the high energy state, known as the Rabi formula,

$$P(t) = \frac{1}{2}(1 - 2s_3(t)) = \frac{1}{1 + D^2} \sin^2\left(\frac{\Omega_R}{2}t\right), \tag{3.8}$$

where

$$D = \left|\frac{k_R - \omega_R}{A_R}\right|. \tag{3.9}$$

is the relative detuning.

The resonance of Rabi oscillations occurs when $\vec{H}'_3 = 0$ in the corotating frame and $\vec{s}$ oscillates between $+1/2$ (the low energy state) and $-1/2$ (the high energy state). The transition amplitude is determined by relative detuning D as illustrated by two numerical examples in Fig. 3.3. The resonance width is determined by the amplitude of the driving field A_R as shown in Fig. 3.4.

In many cases, the two-level quantum system has more than one driving fields. I will refer to each of the driving field as a Rabi mode. Here I consider the Hamiltonian with two Rabi modes:

$$\begin{aligned} \mathsf{H}_R = &-\frac{\omega_R}{2}\sigma_3 - \frac{A_1}{2}\left(\cos(k_1 t + \phi_1)\sigma_1 - \sin(k_1 t + \phi_1)\sigma_2\right) \\ &-\frac{A_2}{2}\left(\cos(k_2 t + \phi_2)\sigma_1 - \sin(k_2 t + \phi_2)\sigma_2\right). \end{aligned} \tag{3.10}$$
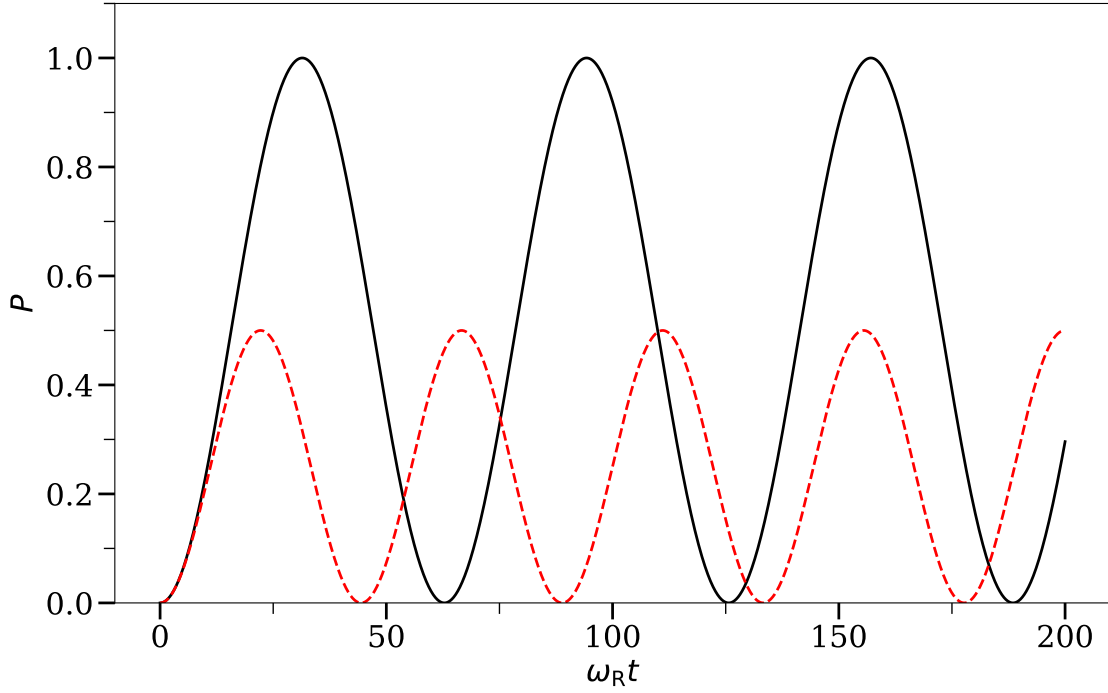
Figure 3.3: The transition probabilities P between the energy states of a two-level quantum system when external driving fields with frequencies $k_{\mathrm{R}} = \omega_{\mathrm{R}}$ and $k_{\mathrm{R}} = 1.1\omega_{\mathrm{R}}$ are applied, respectively. The corresponding relative detunings are $D = 0$ and $D = 1$, respectively. The amplitudes of the driving fields are $A_{\mathrm{R}} = 0.1\omega_{\mathrm{R}}$ in both cases.

I decompose it into $\vec{H}_{\mathrm{R}} = \vec{H}_3 + \vec{H}_1 + \vec{H}_2$, where

$$\vec{H}_1 = \begin{pmatrix} A_1 \cos(k_1 t + \phi_1) \\ -A_1 \sin(k_1 t + \phi_1) \\ 0 \end{pmatrix} \quad \text{and} \quad \vec{H}_2 = \begin{pmatrix} A_2 \cos(k_2 t + \phi_2) \\ -A_2 \sin(k_2 t + \phi_2) \\ 0 \end{pmatrix}.$$

I will assume that the first Rabi mode $\vec{H}_1$ is almost on resonance, and the second one $\vec{H}_2$ is off resonance, i.e.,

$$D_1 \lesssim 1 \quad \text{and} \quad D_2 \gg 1, \tag{3.11}$$

where

$$D_i \equiv \frac{|k_i - \omega_{\mathrm{R}}|}{|A_i|} \tag{3.12}$$

is the relative detuning of the ith Rabi mode.
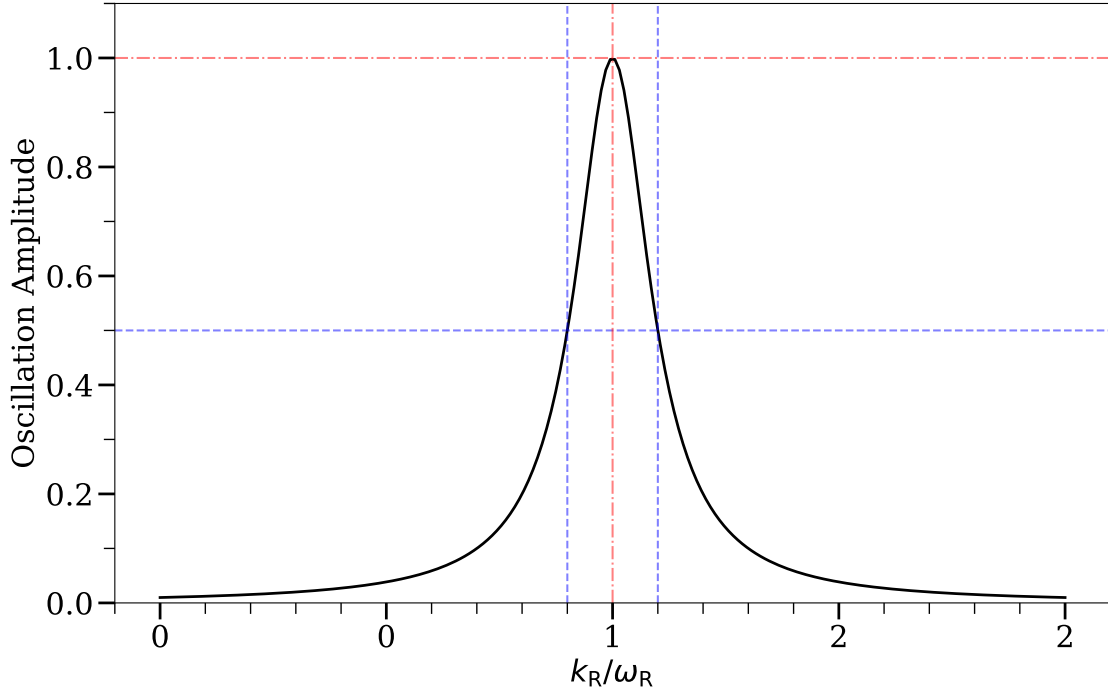
Figure 3.4: The amplitude of Rabi oscillations as a function of the frequency of the external driving field k_{R}. The maximum amplitude occurs at $k_{\mathrm{R}}/\omega_{\mathrm{R}} = 1$. The resonance width is defined to be the difference of k_{R} at which the amplitudes are $1/2$.

Although the second Rabi mode is off resonance, it can interfere with the Rabi oscillation caused by the first Rabi mode. To see this effect, I will use the frame that corotates with $\vec{H}_2$. In the corotating frame, the two Rabi modes have frequencies $k_1' = k_1 - k_2$ and $k_2' = 0$, respectively, and $\vec{H}_3' = (0, 0, \omega_{\mathrm{R}} - k_2)^{\mathrm{T}}$. Obviously, the Hamiltonian vector in this corotating frame is similar to Eqn. 3.1 except with the replacements

$$\vec{H}_3 \to \vec{H}_3' + \vec{H}_2' \quad \text{and} \quad \vec{H}_+ \to \vec{H}_1'. \tag{3.13}$$

I will further assume that $|A_2| \ll \omega_{\mathrm{R}}$ so that the new energy gap is

$$\begin{aligned}
\tilde{\omega}_{\mathrm{R}}' &\equiv |\vec{H}_3' + \vec{H}_2'| \\
&= \mathrm{sign}(\omega_{\mathrm{R}} - k_2)\sqrt{(\omega_{\mathrm{R}} - k_2)^2 + A_2^2} \\
&\approx \omega_{\mathrm{R}} - k_2 + \frac{1}{2}\frac{A_2^2}{\omega_{\mathrm{R}} - k_2},
\end{aligned} \tag{3.14}$$

where I kept only up to the first order of the Taylor series. I can calculate the new

relative detuning of the system to be

$$D' = \frac{|k_1' - \tilde{\omega}_R'|}{|A_1|}$$

$$\approx \left| \frac{k_1 - \omega_R}{A_1} + \frac{A_2^2}{2A_1(k_2 - \omega_R)} \right|. \tag{3.15}$$

One can adjust frequency of the off-resonance Rabi mode k_2 to decrease or increase D so that the system is close to or further away from the resonance. The criterion for the off-resonance Rabi mode to have a significant impact on the Rabi resonance is

$$\left| \frac{A_2^2}{2A_1(k_2 - \omega_R)} \right| \gtrsim 1 \quad \text{or} \quad |A_2| \gtrsim \sqrt{2|A_1(k_2 - \omega_R)|} \tag{3.16}$$

3.2 Background Matter Basis

For a uniform matter density $\lambda(r) = \lambda_0$, one can define a matter basis in which the Hamiltonian is diagonalized:

$$\mathsf{H}^{(\mathrm{m})} = \mathsf{U}^\dagger \mathsf{H}^{(\mathrm{f})} \mathsf{U} = -\frac{\omega_\mathrm{m}}{2} \sigma_3, \tag{3.17}$$

where

$$\mathsf{U} = \begin{pmatrix} \cos\theta_\mathrm{m} & \sin\theta_\mathrm{m} \\ \sin\theta_\mathrm{m} & \cos\theta_\mathrm{m} \end{pmatrix} \tag{3.18}$$

with

$$\theta_\mathrm{m} = \frac{1}{2} \arctan\left(\frac{\sin 2\theta_\mathrm{v}}{\cos 2\theta_\mathrm{v} - \lambda_0/\omega_\mathrm{v}} \right),$$

and

$$\omega_\mathrm{m} = \omega_\mathrm{v} \sqrt{(\lambda_0/\omega_\mathrm{v} - \cos(2\theta_\mathrm{v}))^2 + \sin^2(2\theta_\mathrm{v})} \tag{3.19}$$

is the neutrino oscillation frequency in matter.

In the rest of the chapter, I will consider profiles of the form

$$\lambda(r) = \lambda_0 + \delta\lambda(r), \tag{3.20}$$

where $\delta\lambda(r)$ describes the fluctuation of the matter density. I will use the background matter basis defined in Eqn. 3.2 and Eqn. 3.19. In this basis, the Hamiltonian reads

$$\mathsf{H}^{(\mathrm{m})} = -\frac{\omega_{\mathrm{m}}}{2}\sigma_3 + \frac{1}{2}\delta\lambda(r)\cos 2\theta_{\mathrm{m}}\sigma_3 - \frac{1}{2}\delta\lambda(r)\sin 2\theta_{\mathrm{m}}\sigma_1. \tag{3.21}$$

In this chapter, I will focus on the transition probability between the background matter eigenstates

$$\begin{pmatrix} |\nu_{\mathrm{L}}\rangle \\ |\nu_{\mathrm{H}}\rangle \end{pmatrix} = \mathsf{U}^{\dagger}\begin{pmatrix} |\nu_{\mathrm{e}}\rangle \\ |\nu_{\mathrm{x}}\rangle \end{pmatrix}. \tag{3.22}$$

Given this transition probability, it is trivial to calculate the flavor conversion.

All the numerical examples in this chapter are calculated with $\sin^2(2\theta_{\mathrm{v}}) = 0.093$ and $\omega_{\mathrm{v}} = 3.75 \times 10^{-17}\mathrm{MeV}^2$.

3.3   Single-Frequency Matter Profile

I will examine the neutrino flavor conversion in a single-frequency matter profile $\delta\lambda(r) = \lambda_1\cos(k_1 r)$. I will assume that the perturbation is small so that $\lambda_1 \ll \omega_{\mathrm{m}}$. The Hamiltonian in the background matter basis becomes

$$\mathsf{H}^{(\mathrm{m})} = -\frac{\omega_{\mathrm{m}}}{2}\sigma_3 + \frac{1}{2}\lambda_1\cos(k_1 r)\cos 2\theta_{\mathrm{m}}\sigma_3 - \frac{1}{2}\lambda_1\cos(k_1 r)\sin 2\theta_{\mathrm{m}}\sigma_1. \tag{3.23}$$

I will consider the case when k_1 is not far away from resonance, i.e., $k_1 \sim \omega_{\mathrm{m}}$. As will be proven later, the oscillating σ_3 term $\frac{1}{2}\lambda_1\cos(k_1 r)\cos 2\theta_{\mathrm{m}}\sigma_3$ in the above Hamiltonian has little effect on the transition probabilities in this case. With the oscillating σ_3 term removed,

$$\begin{aligned} \mathsf{H}^{(\mathrm{m})} \to -\frac{\omega_{\mathrm{m}}}{2}\sigma_3 &- \frac{1}{2}A_1\cos(k_1 r)\sigma_1 + \frac{1}{2}A_1\sin(k_1 r)\sigma_2 \\ &- \frac{1}{2}A_2\cos(k_2 r)\sigma_1 + \frac{1}{2}A_2\sin(k_2 r)\sigma_2 \end{aligned} \tag{3.24}$$

where

$$A_1 = A_2 = \frac{\lambda_1\sin(2\theta_{\mathrm{m}})}{2} \quad \text{and} \quad k_2 = -k_1. \tag{3.25}$$

This is the same as the Hamiltonian $\mathsf{H}_{(\mathrm{R})}$ in Eqn. 3.10. Because the second Rabi mode is off resonance and its amplitude is too small to satisfy the criterion in Eqn. 3.16,

it can be neglected and Rabi formula in Eqn. 3.8 can be applied with $A_R = A_1$, $k_R = k_1$, and $\omega_R = \omega_m$.

I calculated the transition probability using the Hamiltonian in Eqn. 3.23 with $k_1/\omega_m = 1$ and plotted it as black square markers in Fig. 3.5. As comparison I also plotted the transition probability obtained from the Rabi formula in Eqn. 3.8 as the dot-dashed curve in the same figure, which agrees with the numerical result very well. In this case, the first Rabi mode is exactly on resonance with relative detuning $D_1 = 0$. I calculated the transition probabilities for additional two cases with $k_1/\omega_m = 1 - 2 \times 10^{-5}$ and $1 - 10^{-4}$, which have relative detunings $D_1 = 1$ and 5.2, respectively. The Rabi resonance is suppressed as D_1 increases. The results obtained using the full Hamiltonian and those from the Rabi formula again agree very well.

For a single-frequency perturbation in the matter profile $\lambda(r) = \lambda_0 + \lambda_1 \sin(k_1 r)$, P. Krastev and A. Smirnov concluded that the parametric resonance condition is $\omega_m \sim n k_1$, if

$$\omega_{m,\text{inst}}(r) = \omega_v \sqrt{(\lambda(r)/\omega_v - \cos(2\theta_v))^2 + \sin^2(2\theta_v)} \tag{3.26}$$

varies slowly with r [7]. This condition is exactly the Rabi resonance condition when $n = 1$. Higher order effects will be explained in Sec. 3.6.

3.4 Multi-Frequency Matter Profiles

The approach applied to the neutrino flavor transformation with a single-frequency matter profile can also be used in more general cases with multi-frequency matter profiles. Even though there is only one Rabi mode that is on resonance, the presence of many off-resonance Rabi modes may interfere with the on-resonance mode and suppress or enhance the neutrino flavor conversion.

I will consider a matter profile with two Fourier modes:

$$\lambda(r) = \lambda_0 + \lambda_1 \cos(k_1 r) + \lambda_2 \cos(k_2 r). \tag{3.27}$$
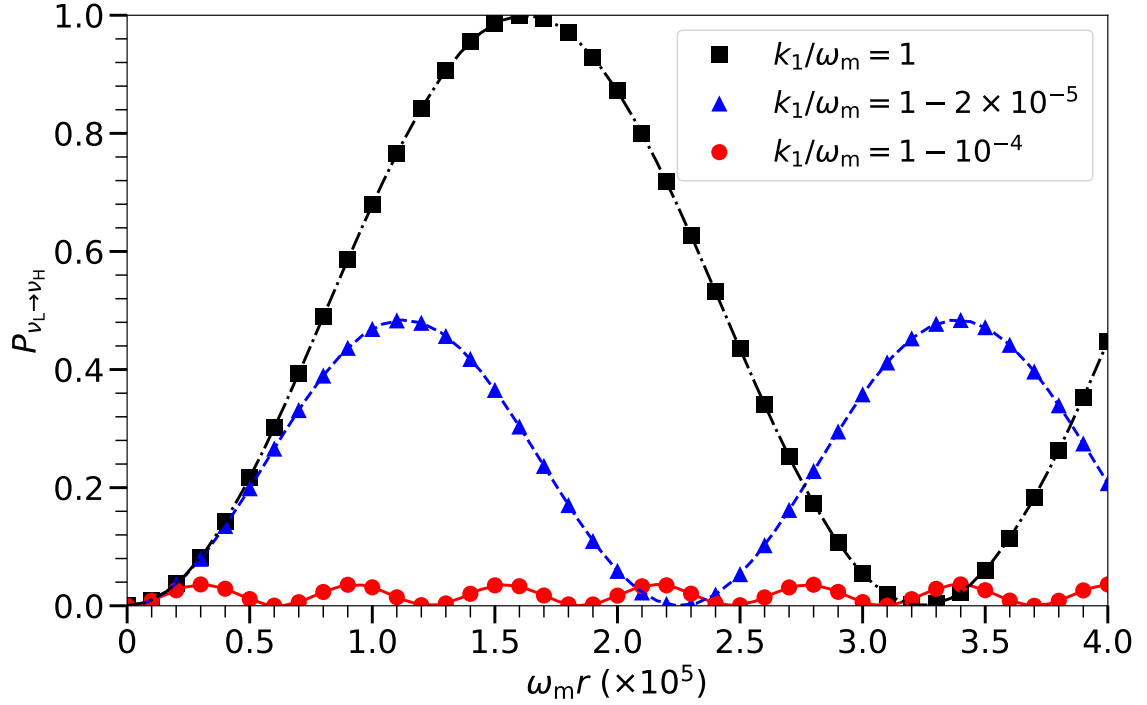
Figure 3.5: The transition probabilities $P_{\nu_L \to \nu_H}$ as functions of distance r for a neutrino propagating through matter profiles $\lambda(r) = \lambda_0 + \lambda_1 \cos(k_1 r)$ with different values of k_1 as labeled. The markers are for the numerical results obtained by using the Hamiltonian in Eqn. 3.23, and the continuous curves are obtained using the Rabi formula in Eqn. 3.8. In all three cases, λ_0 is half of the MSW resonance potential, and $\lambda_1/\omega_m = 5.2 \times 10^{-4}$.

The Hamiltonian for the neutrino oscillations in the background matter basis is

$$
\begin{aligned}
\mathsf{H}^{(\mathrm{m})} = {} & -\frac{\omega_{\mathrm{m}}}{2}\sigma_3 + \frac{1}{2}\left(\lambda_1 \cos(k_1 r) + \lambda_2 \cos(k_2 r)\right)\cos 2\theta_{\mathrm{m}}\sigma_3 \\
& -\frac{1}{2}\left(\lambda_1 \cos(k_1 r) + \lambda_2 \cos(k_2 r)\right)\sin 2\theta_{\mathrm{m}}\sigma_1.
\end{aligned} \tag{3.28}
$$

I will drop the oscillating σ_3 terms for the same reason as in the single-frequency matter profile case. The Hamiltonian becomes

$$
\mathsf{H}^{(\mathrm{m})} \to -\frac{\omega_{\mathrm{m}}}{2}\sigma_3 - \sum_n \frac{A_n}{2}\cos(k_n r)\sigma_1 + \sum_n \frac{A_n}{2}\sin(k_n r)\sigma_2. \tag{3.29}
$$

There are four Rabi modes in this Hamiltonian, $n = 1+$, $1-$, $2+$, and $2-$. The

amplitudes and wave numbers of the four Rabi modes are

$$A_{1\pm} = \frac{\lambda_1 \sin(2\theta_{\mathrm{m}})}{2}, \qquad\qquad k_{1\pm} = \pm k_1, \qquad (3.30)$$

$$A_{2\pm} = \frac{\lambda_2 \sin(2\theta_{\mathrm{m}})}{2}, \qquad\qquad k_{2\pm} = \pm k_2, \qquad (3.31)$$

respectively.
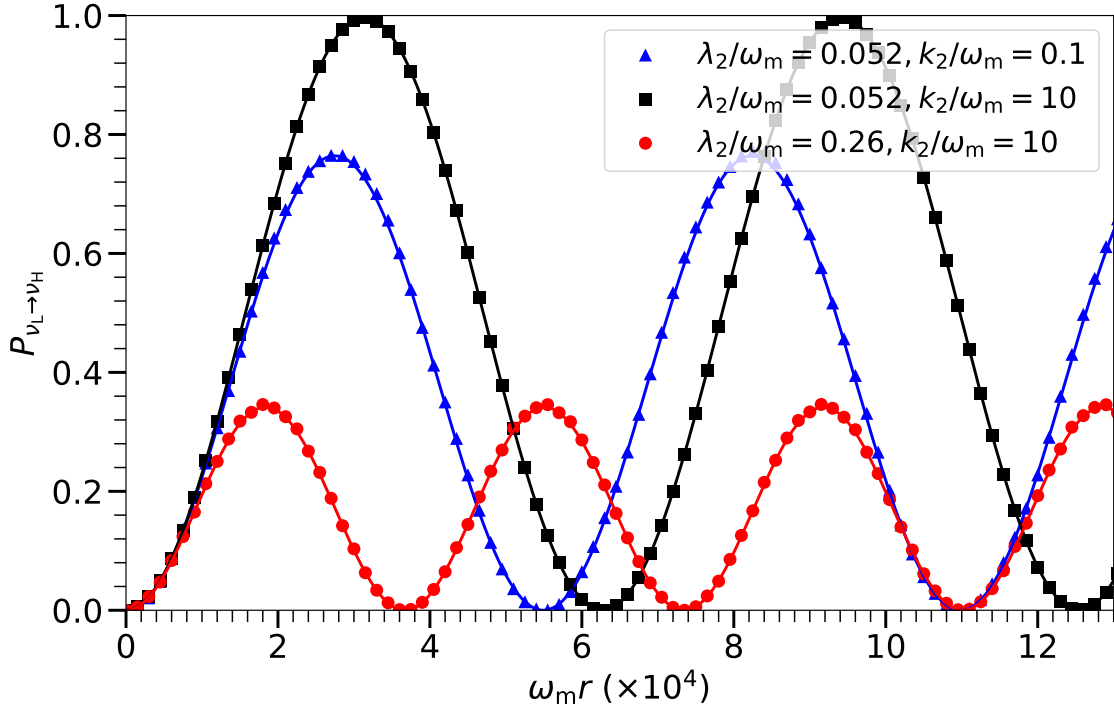
Figure 3.6: The transition probabilities as functions of distance r for a neutrino propagating through matter profile $\lambda(r) = \lambda_0 + \lambda_1 \cos(k_1 r) + \lambda_2 \cos(k_2 r)$ with different values of λ_2 and k_2 as labeled. The markers are for the numerical results obtained by using the Hamiltonian in Eqn. 3.28, and the continuous curves are obtained using the Rabi formula in Eqn. 3.8 but with the values of the modified relative detunings D'_{2+} in Table 3.1. In all three cases, λ_0 is half of the MSW resonance potential, $\lambda_1/\omega_{\mathrm{m}} = 5.2 \times 10^{-4}$ and $k_1/\omega_{\mathrm{m}} = 1$.

The presence of the additional Fourier mode can suppress the Rabi resonance. This is illustrated in Fig. 3.6. In this figure, I choose the 1+ Rabi mode to be exactly on resonance with $\lambda_1/\omega_{\mathrm{m}} = 5.2 \times 10^{-4}$ and $k_1/\omega_{\mathrm{m}} = 1$. The triangles represent the numerical solution for neutrino flavor transformation with $\lambda_2/\omega_{\mathrm{m}} = 0.052$ and $k_2/\omega_{\mathrm{m}} = 0.1$. One can see that the transition amplitude is suppressed due to the presence of the second Fourier mode. I used Eqn. 3.15 to calculate the modified

$\lambda_2/\omega_{\mathrm{m}}$	k_2/ω_{m}	D'_{1-}	D'_{2+}	D'_{2-}
0.052	0.1	2.5×10^{-5}	0.56	0.46
0.052	10	2.5×10^{-5}	0.056	0.045
0.26	10	2.5×10^{-5}	1.4	1.1

Table 3.1: The relative detunings of the Rabi resonance when only the 1+ mode and another Rabi mode are considered.

relative detunings by taking into account only the 1+ mode and another Rabi mode. The values of the relative detunings are listed in Table 3.1. I calculated the transition probability using the Rabi formula in Eqn. 3.8 with the relative detuning D'_{2+} (the continuous curve in the figure, and it agrees with the numerical solution very well. I also showed two additional examples with $(\lambda_2/\omega_{\mathrm{m}}, k_2/\omega_{\mathrm{m}})$ being $(0.052, 10)$ and $(0.26, 10)$, respectively. In both examples, the numerical solutions and the analytic results by using the Rabi formula have excellent agreement.

The presence of the second Fourier mode can also enhance the Rabi resonance, which is illustrated in Fig. 3.7. The two Fourier modes in this figure have amplitudes and wave numbers

$$\lambda_1/\omega_{\mathrm{m}} = 5.2 \times 10^{-4}, \qquad\qquad k_1/\omega_{\mathrm{m}} = 1 - 10^{-4},$$
$$\lambda_2/\omega_{\mathrm{m}} = 0.1, \qquad\qquad k_2/\omega_{\mathrm{m}} = 3,$$

respectively. The neutrino flavor conversion is never complete if only the first Fourier mode is present because the relative detunign $D_{1+} = 1 > 0$. This is shown as the red dots in the figure. However, complete neutrino flavor conversion when both Fourier modes are present. This is because the modified relative detuning $D'_{2+} = 0$ when only the 1+ and the 2+ Rabi modes are considered. The numerical solution and the analytic prediction using the Rabi formula are plotted as the black squares and the continuous curve, respectively, which agree very well.
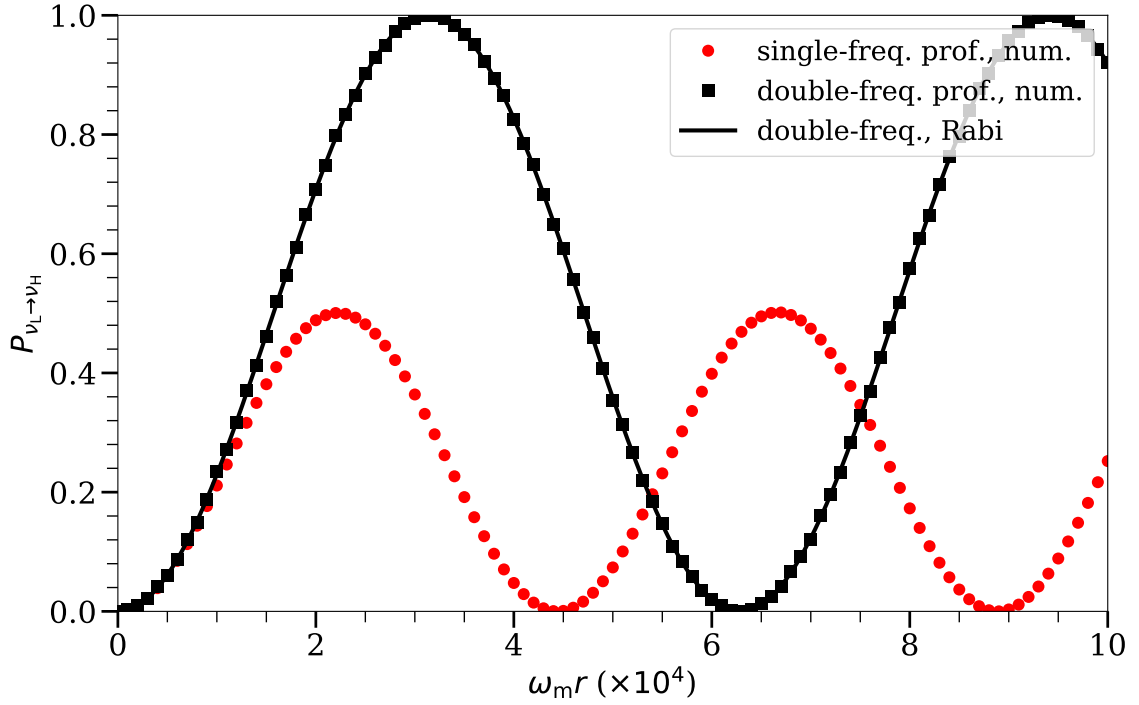
Figure 3.7: The constructive interference effect for the neutrino flavor conversion with a two-frequency matter density profile as in Fig. 3.6. The red dots represent the numerical solution in the case of a single-frequency matter profile with $\lambda_1/\omega_{\mathrm{m}} = 5.2 \times 10^{-4}$ and $k_1/\omega_{\mathrm{m}} = 1 - 10^{-4}$. The black square markers represent the numerical solution with an additional Fourier mode with $\lambda_2/\omega_{\mathrm{m}} = 0.1$ and $k_2/\omega_{\mathrm{m}} = 3$. The black curve is obtained using the Rabi formula in Eqn. 3.8 with relative detuning $D'_{2+} = 0$.

3.5 Rabi Basis

Previously I have ignored the oscillating σ_3 terms in the Hamiltonian such as in Eqn. 3.23. Using the Jacobi-Anger expansion, J. Kneller et al. showed that these terms result in an infinite number of resonance conditions. In the rest of the chapter, I will present a much simpler derivation of their results from the perspective of Rabi oscillations. For this purpose I will define a new basis called Rabi basis

$$\begin{pmatrix} |\nu_{\mathrm{r}1}\rangle \\ |\nu_{\mathrm{r}2}\rangle \end{pmatrix} = \mathsf{U}^\dagger \begin{pmatrix} |\nu_{\mathrm{L}}\rangle \\ |\nu_{\mathrm{H}}\rangle \end{pmatrix}, \tag{3.32}$$

where

$$U = \begin{pmatrix} e^{-i\eta(r)} & 0 \\ 0 & e^{i\eta(r)} \end{pmatrix}. \tag{3.33}$$

The unitary transformation in Eqn. 3.33 is a rotation in flavor space about the third axis. It commutes with σ_3 terms in the Hamiltonian, but, due to its dependence on r, the left side of the Schrödinger equation obtains an extra term:

$$\begin{pmatrix} \frac{d\eta}{dr} & 0 \\ 0 & -\frac{d\eta}{dr} \end{pmatrix} \begin{pmatrix} \psi_{R1} \\ \psi_{R2} \end{pmatrix} + i \frac{d}{dr} \begin{pmatrix} \psi_{R1} \\ \psi_{R2} \end{pmatrix}$$
$$= \left[-\frac{\omega_m}{2}\sigma_3 + \frac{\delta\lambda}{2}\cos 2\theta_m \sigma_3 - \frac{\delta\lambda}{2}\sin 2\theta_m \begin{pmatrix} 0 & e^{2i\eta} \\ e^{-2i\eta} & 0 \end{pmatrix} \right] \begin{pmatrix} \psi_{R1} \\ \psi_{R2} \end{pmatrix}.$$

The oscillating σ_3 terms in Hamiltonian can be eliminated by choosing $\eta(r)$ properly, i.e.,

$$\eta(r) - \eta(0) = \frac{\cos 2\theta_m}{2} \int_0^r \delta\lambda(\tau)d\tau. \tag{3.34}$$

With this definition, the Schrödinger equation simplifies:

$$i\frac{d}{dr} \begin{pmatrix} \psi_{r1} \\ \psi_{r2} \end{pmatrix} = \left[-\frac{\omega_m}{2}\sigma_3 - \frac{\delta\lambda}{2}\sin 2\theta_m \begin{pmatrix} 0 & e^{2i\eta} \\ e^{-2i\eta} & 0 \end{pmatrix} \right] \begin{pmatrix} \psi_{r1} \\ \psi_{r2} \end{pmatrix}. \tag{3.35}$$

Because the states $|\nu_{r1}\rangle$ and $|\nu_{r2}\rangle$ are related to $|\nu_L\rangle$ and $|\nu_H\rangle$ by phase factors only, the transition probability between the former two states is the same as that between the latter.

3.6 Single-Frequency Matter Profile Revisited

Let us consider the single-frequency matter profile that we have studied in Sec. 3.3 again. In the Rabi basis, the Hamiltonian becomes

$$H^{(R)} = \frac{\omega_m}{2}\sigma_3 - \frac{\sin 2\theta_m \lambda_1 \cos(k_1 r)}{2} \begin{pmatrix} 0 & e^{2i\eta(r)} \\ e^{-2i\eta(r)} & 0 \end{pmatrix}, \tag{3.36}$$

where

$$\eta(r) = \frac{\lambda_1 \cos 2\theta_m}{2k} \sin(k_1 r). \tag{3.37}$$

With the Jacobi-Anger expansion

$$e^{iz\sin(\phi)} = \sum_{n=-\infty}^{\infty} J_n(z)e^{in\phi}, \tag{3.38}$$

the term $e^{2i\eta(r)}$ becomes

$$\exp\left(i\frac{\lambda_1\cos 2\theta_{\rm m}}{k_1}\sin(k_1 r)\right) = \sum_{n=-\infty}^{\infty} J_n\left(\frac{\lambda_1\cos 2\theta_{\rm m}}{k_1}\right)e^{ink_1 r}, \tag{3.39}$$

and the Hamiltonian becomes a Rabi oscillation system with infinite number of Rabi modes:

$$\mathsf{H}^{(\rm R)} = -\frac{\omega_{\rm m}}{2}\sigma_3 - \frac{1}{2}\sum_{n=-\infty}^{\infty} A_n\begin{pmatrix} 0 & e^{ink_1 r} \\ e^{-ink_1 r} & 0 \end{pmatrix}, \tag{3.40}$$

where $J_n(z)$ is the Bessel function of the first kind of order n, and

$$A_n = \tan 2\theta_{\rm m} n k_1 J_n\left(\frac{\lambda_1}{k_1}\cos 2\theta_{\rm m}\right) \tag{3.41}$$

and nk_1 are the amplitude and wave number of the nth Rabi mode.[1] In obtaining Eqn. 3.40, I have used the following identify of the Bessel function

$$J_{n-1}(z) + J_{n+1}(z) = \frac{2n}{z}J_n(z). \tag{3.42}$$

Eqn. 3.40 implies an infinite number of resonance conditions

$$\omega_{\rm m} = nk_1 \qquad (n = 1, 2, \ldots) \tag{3.43}$$

However, the amplitude of the Rabi mode A_n drops quickly as a function of n because

$$J_n(z) \xrightarrow{z \ll \sqrt{n+1}} \frac{(z/2)^n}{n!} \qquad \text{if } n > 0 \tag{3.44}$$

when $\lambda_1/k_1 \ll 1$. For $\lambda_1/k_1 \gtrsim 1$, A_n also becomes small for sufficiently large n because

$$J_n(z) \xrightarrow{n \gg 1} \frac{1}{\sqrt{2\pi n}}\left(\frac{ez}{2n}\right)^n. \tag{3.45}$$

Any real physical system has a finite size l and the Rabi modes with the oscillation wavelengths $2\pi/\Omega_n \sim 2\pi/A_n \gtrsim l$ can be ignored even if they are on resonance.

---

[1] A phase in the matter potential would contribute to the phases of the Rabi modes which do not play any role in the resonance for the reason discussed in Sec. 3.1

	$k_1/\omega_{\mathrm{m}} = 1$			$k_1/\omega_{\mathrm{m}} = 1 - 2 \times 10^{-5}$			$k_1/\omega_{\mathrm{m}} = 1 - 10^{-4}$		
n	A_n/A_1	D_n	$\Delta D_{(n)}$	A_n/A_1	D_n	$\Delta D_{(n)}$	A_n/A_1	D_n	$\Delta D_{(n)}$
-1	1	10^5	5×10^{-6}	1	10^5	5×10^{-6}	1	10^5	5×10^{-6}
2	4.8×10^{-5}	1.1×10^9	2.2×10^{-14}	4.8×10^{-5}	1.1×10^9	2.2×10^{-14}	4.8×10^{-5}	1.1×10^9	2.2×10^{-14}
-2	4.8×10^{-5}	3.2×10^9	7.5×10^{-15}	4.8×10^{-5}	3.2×10^9	7.5×10^{-15}	4.8×10^{-5}	3.2×10^9	7.6×10^{-15}

Table 3.2: The amplitudes and the relative detunings of a few Rabi modes and their impact on the Rabi resonance for the three numerical examples shown in Fig. 3.5.

In Sec. 3.3, I have discussed the scenario where the $n = 1$ Rabi mode is on or close to resonance and $\lambda_1/\omega_{\mathrm{m}} \ll 1$. Using Eqn. 3.44 and identity

$$J_{-n}(z) = (-1)^n J_n(z) \tag{3.46}$$

I obtain

$$A_{\pm 1} \approx \frac{\lambda_1 \sin(2\theta_{\mathrm{m}})}{2}, \tag{3.47}$$

which agrees with Eqn. 3.25. According to Eqn. 3.15, compared with the case where the first Rabi mode is present, the relative detuning of the Rabi resonance has a change of magnitude

$$\Delta D_{(n)} = \frac{1}{2} \frac{A_n}{A_1} \frac{1}{D_n} \tag{3.48}$$

when another Rabi mode n is present, where D_n is the relative detuning when only the nth Rabi mode is considered. In Table 3.2, I listed the values of A_n/A_1, D_n, and $\Delta D_{(n)}$ of a few off-resonance Rabi modes for the three numerical examples plotted in Fig. 3.5. One can see that all the off-resonance Rabi modes have very little impact on the resonance which explains why we could ignore the oscillating σ_3 terms in Eqn. 3.24.

3.7 Multi-frequency Matter Profile Revisited

For a multi-frequency matter profile

$$\lambda(r) = \lambda_0 + \sum_a \lambda_a \cos(k_a r), \tag{3.49}$$

it is straightforward although a little bit tedious to show that the Hamiltonian in the Rabi basis is

$$\mathsf{H}^{(\mathrm{R})} = -\frac{\omega_{\mathrm{m}}}{2}\sigma_3 - \frac{1}{2}\sum_{\{n_a\}} A_{\{n_a\}} \begin{pmatrix} 0 & e^{iK_{\{n_a\}}r} \\ e^{-iK_{\{n_a\}}r} & 0 \end{pmatrix}, \tag{3.50}$$

where $\{n_a\}$ stands for a set of arbitrary integers each associating with a particular Fourier mode, and

$$K_{\{n_a\}} = \sum_a n_a k_a \tag{3.51}$$

and

$$A_{\{n_a\}} = \tan(2\theta_{\mathrm{m}})K_{\{n_a\}} \prod_a J_{n_a}\left(\frac{\lambda_a}{k_a}\cos(2\theta_{\mathrm{m}})\right). \tag{3.52}$$

are the wave number and amplitude of the Rabi mode denoted by $\{n_a\}$, respectively. There are potentially many Rabi modes that approximately satisfy the resonance condition

$$K_{\{n_a\}} = \omega_{\mathrm{m}}. \tag{3.53}$$

However, according to the discussion in Sec. 3.6, the Rabi modes with large $|n_a|$s have very long oscillation wavelengths and can be ignored even if they are on resonance. The off-resonance Rabi modes with large $|n_a|$s have very small amplitudes and do not have a significant impact on the resonance either. Therefore, only a finite number of Rabi modes need to be considered for a realistic system.

As an example of a matter profile with multiple frequencies, I will consider the castle wall profile

$$\lambda(r) = \begin{cases} \Lambda_1 & \text{if } -\frac{X_1}{2} + nX \leq r \leq \frac{X_1}{2} + nX, \\ \Lambda_2 & \text{otherwise}, \end{cases} \tag{3.54}$$

where n is arbitrary integer, X is the period of the potential, and Λ_1, Λ_2, and X_1 are constants. The parametric resonance condition for the castle wall potential has been derived by E. Akhmedov [12]:

$$\frac{\tan(\omega_{\mathrm{m1}}X_1/2)}{\tan(\omega_{\mathrm{m2}}X_2/2)} = -\frac{\cos 2\theta_{\mathrm{m2}}}{\cos 2\theta_{\mathrm{m1}}}, \tag{3.55}$$

where

$$\omega_{\mathrm{m}i} = \omega_{\mathrm{v}}\sqrt{(\Lambda_i/\omega_{\mathrm{v}} - \cos(2\theta_{\mathrm{v}}))^2 + \sin^2 2\theta_{\mathrm{m}}}, \tag{3.56}$$

$$\theta_{\mathrm{m}i} = \frac{1}{2}\arctan\left(\frac{\sin(2\theta_{\mathrm{v}})}{\cos(2\theta_{\mathrm{v}}) - \Lambda_i/\omega_{\mathrm{v}}}\right) \tag{3.57}$$

and $X_2 = X_1$. To study the parametric resonance with this particular matter profile, I will decompose the profile into a Fourier series:

$$\lambda(r) = \lambda_0 + \sum_{a=1}^{\infty} \lambda_a \cos\left(k_a r\right), \tag{3.58}$$

where I have assumed $X_1 = X_2 = X/2$,

$$\lambda_0 = (\Lambda_1 + \Lambda_2)/2,$$
$$\lambda_a = \frac{2}{(2a-1)\pi}(-1)^a\left(\Lambda_1 - \Lambda_2\right),$$
$$k_a = (2a-1)k_1,$$
$$k_1 = 2\pi/X.$$

As a concrete example, I choose $\Lambda_1 = 0.3\omega_{\mathrm{v}}\cos(2\theta_{\mathrm{v}})$, $\Lambda_2 = 0.7\omega_{\mathrm{v}}\cos(2\theta_{\mathrm{v}})$, and $X = 2\pi/\omega_{\mathrm{m}}$. For this particular example, the Rabi mode $\{1, 0, 0, \cdots\}$ is on resonance. In Fig. 3.8, I compared the numerical solution to the full equation of motion and that obtained from the Rabi formula in Eqn. 3.8. They agree with each other very well.

In the above example, there are an infinite number of Rabi modes that are on resonance in addition to $\{1, 0, 0, \cdots\}$. In principle, one should add the amplitudes of all these resonances modes together in calculating the transition probability with the Rabi formula. However, all the Rabi modes that on resonance have very tiny amplitudes except $\{1, 0, 0, \cdots\}$ (see Table. 3.3), therefore they can be neglected in calculations. There are also an infinite number of Rabi modes that off resonance. In Table. 3.3 I listed some of these Rabi modes with the largest amplitudes. One can see that the change to the relative detunings $D_{(\{n_a\})}$ of the on-resonance mode $\{1, 0, 0, \cdots\}$ due to the presence of the mode $\{n_a\}$ are all very small. As a result, they all have very little impact on the neutrino flavor conversion. This explains the
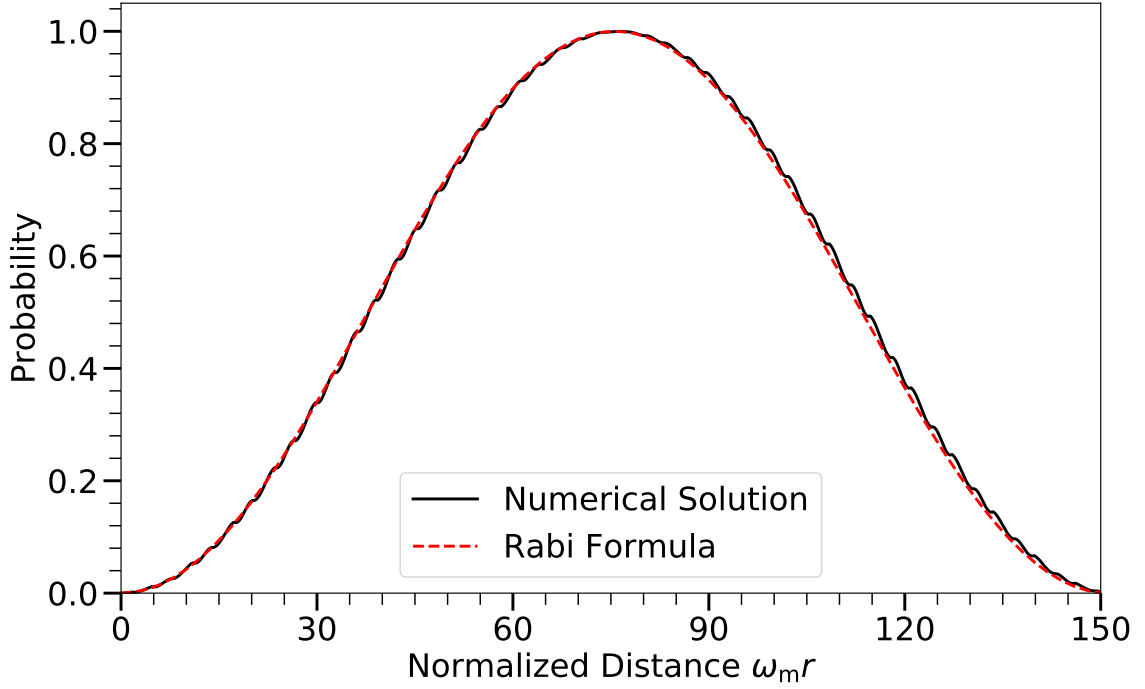
Figure 3.8: The transition probabilities of neutrino flavor conversion with a castle wall matter profile as functions of distance r. The period of the castle wall potential X is chosen that the Rabi mode with wave number $K = 1$ is on resonance.

agreement between the numerical solution and the result using the Rabi formula in Fig. 3.8.

$\{n_a\}$	$A_{\{n_a\}}/A_{\{1,0,0,\cdots\}}$	$D_{\{n_a\}}$	$\Delta D_{(\{n_a\})}$
$\{-2,1,0,\cdots\}$	5.4×10^{-4}	0	-
$\{-1,-1,1,\cdots\}$	4.3×10^{-5}	0	-
$\{0,2,-1,\cdots\}$	2.4×10^{-6}	0	-
$\{-1,0,0,\cdots\}$	1	48	1.0×10^{-2}
$\{0,1,0,\cdots\}$	0.33	1.5×10^2	1.1×10^{-3}
$\{2,0,0,\cdots\}$	1.3×10^{-3}	2.4×10^2	2.0×10^{-4}

Table 3.3: The amplitudes and relative detunings of a few Rabi modes $\{n_a\}$ and the changes to the relative detunings of the on-resonance modes due to these Rabi modes if they are off-resonance.

3.8   Conclusions

In this chapter, I have shown that the flavor conversion of a neutrino can be greatly enhanced when it propagates through a oscillatory matter profile when certain resonance conditions are satisfied. This derivation is done from the perspective of Rabi oscillations and is much more physically intuitive than the original derivation by J. Kneller et al. in references [27, 28]. I have shown that, although there can exist an infinite number of Rabi modes that approximately satisfy the resonance condition, only a few of them need to be considered for a real system. I have also derived a criterion when an off-resonance Rabi mode may significantly affect the resonance. Using this criterion I have shown that only a few of the infinite set of off-resonance Rabi modes may contribute to neutrino flavor conversion. Although I have assumed small perturbations on top of a constant matter profile, this approach can be applied to a matter profile with perturbations on top of a smoothly varying background density as have been done by K. Patton et al. in reference [31]. This result maybe applicable to the regions in a star where the matter density fluctuates. There can also exist a turbulent matter distribution behind the shock in a core-collapse supernova where this result maybe applicable. However, the large neutrino fluxes inside a supernova core may have an even larger impact neutrino oscillations which we will consider in the next chapter.

Chapter 4

Collective Neutrino Oscillations

Neutrino oscillations in the matter background have well defined linear dynamics as I have discussed in the preceding chapters. In this chapter, I will discuss neutrino oscillations in a dense neutrino medium where the equation of motion becomes nonlinear. One of such examples is the (core-collapse) supernova explosion which releases approximately 10^{58} neutrinos within seconds [6]. The neutrino density inside a supernova can be so large that that the neutrino self-interaction potential $H_{\nu\nu}$ to be comparable to or even larger than the matter potential in certain regions [4]. It has been shown that the self-interaction between the neutrinos can cause the neutrino medium to oscillate collectively [15, 21]. The neutrino self-interaction also introduces a new characteristic energy scale which is proportional to the neutrino number density. As a result it is possible that neutrinos can oscillate on distance scales much shorter than the vacuum neutrino oscillation wavelength [32, 35].

In this chapter, I will first review some of the general features of collective neutrino oscillations and introduce the method of linearized flavor stability analysis. I will then discuss the dispersion relation of the collective modes of neutrino oscillations and show that it may or may not be related to the flavor stability of neutrino gas. Finally, I will demonstrate an preliminary study of a toy model which can be used to understand the neutrino oscillations in the presence of the neutrino halo [24, 26].

4.1 Equation of Motion

The equation of motion for neutrino oscillations with self-interaction is[8]

$$i\frac{d}{dt}\rho = [\mathsf{H}, \rho], \tag{4.1}$$

where the total derivative is

$$\frac{d}{dt} = \partial_t + \mathbf{v} \cdot \mathbf{\nabla}, \tag{4.2}$$

and the Hamiltonian Hamiltonian is composed of three different terms:

$$\mathsf{H} = \mathsf{H}_{\mathrm{v}} + \mathsf{H}_{\mathrm{m}} + \mathsf{H}_{\nu\nu}. \tag{4.3}$$

In the above equation, the vacuum Hamiltonian is

$$\mathsf{H}_{\mathrm{v}} = \begin{cases} -\frac{1}{2}\eta\omega_{\mathrm{v}}\sigma_3 & \text{for neutrinos,} \\\\ \frac{1}{2}\eta\omega_{\mathrm{v}}\sigma_3 & \text{for antineutrinos,} \end{cases}$$

and the matter potential is

$$\mathsf{H}_{\mathrm{m}} = \frac{1}{2}\lambda\sigma_3 = \frac{1}{2}\sqrt{2}G_{\mathrm{F}}n_{\mathrm{e}}\sigma_3, \tag{4.4}$$

where $\eta = +1$ for the normal neutrino mass hierarchy and -1 for the inverted neutrino mass hierarchy, ω_{v} is the vacuum oscillation frequency of the neutrino or antineutrino, and n_{e} is the net electron number density. The neutrino self-interaction is more complicated and can be written as

$$\mathsf{H}_{\nu\nu} = \sqrt{2}G_{\mathrm{F}} \int dE' d\Omega_{\mathbf{v}'} \left[n(E', \mathbf{v}')\rho(E', \mathbf{v}') - \bar{n}(E', \mathbf{v}')\bar{\rho}(E', \mathbf{v}') \right] (1 - \mathbf{v} \cdot \mathbf{v}'), \tag{4.5}$$

where $n(E, \mathbf{v})$ and $\rho(E, \mathbf{v})$ are the number density and the flavor density matrix of the neutrino with energy E and velocity $\mathbf{v}$, and $\bar{n}(E, \mathbf{v})$ and $\bar{\rho}(E, \mathbf{v})$ are the corresponding quantities of the antineutrino.

The presence of the neutrino self-interaction potential make the equation of motion 4.1 nonlinear, and many interesting phenomenon arise because of it. For example, a dense neutrino medium can experience synchronized oscillation during which all the neutrinos and antineutrinos oscillate with the same frequency [14, 18, 19,

21]. To see this, I will consider an isotropic and homogeneous neutrino gas and use the flavor isospin picture discussed in Sec. 2.4. The flavor isospin of the neutrino is defined by

$$\rho = \frac{1}{2} + \vec{s} \cdot \vec{\sigma}. \tag{4.6}$$

The equation of motion of the flavor isospin is

$$\dot{\vec{s}} = \vec{s} \times \left(\vec{H}_{\mathrm{v}} + \vec{H}_{\nu\nu} \right), \tag{4.7}$$

where

$$\vec{H}_{\mathrm{v}} = \omega_{\mathrm{v}} \begin{pmatrix} -\sin 2\theta_{\mathrm{v}} \\ 0 \\ \cos 2\theta_{\mathrm{v}} \end{pmatrix} = \omega_{\mathrm{v}} \vec{B}, \tag{4.8}$$

and

$$\vec{H}_{\nu\nu} = \sqrt{2} G_{\mathrm{F}} \int dE' n(E') \vec{s}(E'). \tag{4.9}$$

Here for simplicity I have assumed $n_{\mathrm{e}} = 0$ and $\bar{n} = 0$. When the neutrino density is very large, $\vec{H}_{\nu\nu}$ dominates over $\vec{H}_{\mathrm{v}}$ in Eqn. 4.7, and $\vec{s}_{\mathrm{v}}$ precesses about $\vec{H}_{\nu\nu}$ rapidly. Meanwhile, the total flavor isospin

$$\vec{S} = \int dE' f(E') \vec{s}(E') \tag{4.10}$$

precesses about $\vec{H}_{\mathrm{v}}$ slowly with a mean oscillation frequency $\langle omega_{\mathrm{v}} \rangle$, where

$$f(E) = \frac{n(E)}{\int dE' n(E')} \tag{4.11}$$

is the energy distribution of the neutrino. To see this, one can multiply Eqn. 4.7 by $f(E)$ and integrate over E which gives

$$\dot{\vec{S}} = \int dE f(E) \vec{s}(E) \times \omega_{\mathrm{v}} \vec{B} \tag{4.12}$$

$$\rightarrow \int dE f(E) \left[\frac{\vec{s}(E) \cdot \vec{S}}{|\vec{S}|^2} \vec{S} \right] \times \omega_{\mathrm{v}} \vec{B} \tag{4.13}$$

$$= \langle \omega_{\mathrm{v}} \rangle \vec{S} \times \vec{B}, \tag{4.14}$$

where

$$\langle \omega_{\mathrm{v}} \rangle = \int dE f(E) \left[\frac{\vec{s}(E) \cdot \vec{S}}{|\vec{S}|^2} \right] \omega_{\mathrm{v}}. \tag{4.15}$$

In the above equation I have replaced flavor isospin $\vec{s}$ with its projection along the direction of $\vec{S}$ because its precession about $\vec{S}$ is much faster than the precession of $\vec{S}$ about $\vec{B}$.

4.2   Two-Beam Model and Flavor Instability

During the synchronized flavor transformation, the whole neutrino medium behaves as if there were a single neutrino oscillates with the mean frequency $\langle \omega_{\mathrm{v}} \rangle$ in vacuum. Under certain conditions, the neutrino self-interaction potential can cause the neutrino medium to evolve in a way completely different than the vacuum oscillations. I will illustrate this phenomenon using the two-beam neutrino model.

In the two-beam model, neutrinos and antineutrinos are emitted in two different directions from a plane (which we assume to be the x-y plane) with angles θ_1 and θ_2 as shown in Fig. 4.1. I will assume that the neutrino emission plane is homogeneous and that the neutrino and antineutrino have the same density n in the emission plane. I will also assume that the matter density vanishes everywhere in space.
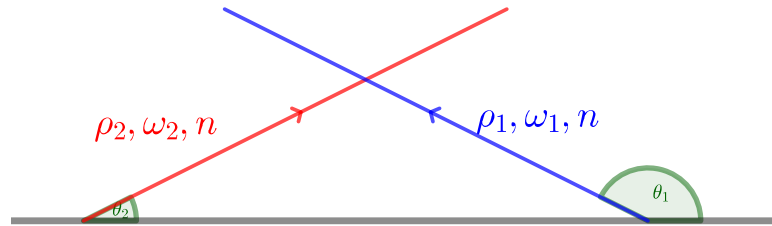
Figure 4.1: The geometry of two-beam model. The ith $(i = 1, 2)$ neutrino beam has emission angle θ_i, vacuum oscillation frequency ω_i and density matrix ρ_i. Both neutrino beams have the same number flux n.

The Hamiltonian of the ith neutrino beam in the vacuum basis is

$$\mathsf{H}_i = -\frac{\omega_i}{2}\sigma_3 + \mu(\rho_1 - \rho_2), \tag{4.16}$$

where $\omega_1 = \eta\omega_{\mathrm{v}}$ for the neutrino beam and $\omega_2 = -\eta\omega_{\mathrm{v}}$ for the antineutrino beam,

$$\mu = \sqrt{2}G_{\mathrm{F}}(1 - \cos(\theta_1 - \theta_2))n \tag{4.17}$$

is the neutrino self-interaction potential.

I will assume that the neutrinos and antineutrino are emitted in the pure electron flavor at $z = 0$. I will also assume the vacuum mixing angle $\theta_{\mathrm{v}} \ll 1$. Therefore, the flavor density matrix of the ith neutrino beam in the vacuum basis at $z = 0$,

$$\rho_i(z = 0) \approx \begin{pmatrix} 1 & \epsilon_i(0) \\ \epsilon_i^*(0) & 0 \end{pmatrix}, \tag{4.18}$$

where

$$\epsilon_i(0) = \sin(2\theta_{\mathrm{v}}) \ll 1. \tag{4.19}$$

I solve the two-beam model numerically with $\epsilon_i = 10^{-3}$ and $\eta = -1$. The solution is shown in Fig. 4.2. When $\omega_{\mathrm{v}}z \ll 1$, the flavor isospin of the neutrino stays in the electron flavor state, i.e., in the direction of third axis $\vec{e}_3$ in the flavor isospin space (see the left panel of Fig. 4.2). Accordingly, the electron flavor survival probability $P_{\nu_{\mathrm{e}}} \approx 1$ at small z but falls down rapidly at a certain value of z (see the right panel of Fig. 4.2). Then both the flavor isospin and $P_{\nu_{\mathrm{e}}}$ come back to their original positions until they fall down again. The flavor isospin of the antineutrino follows a similar pattern but is in a different direction. This flavor transformation phenomenon is clearly different from the vacuum oscillation shown in Fig. 2.1.

To gain a deeper understanding of the collective oscillation phenomenon, I will focus on the linear regime where $|\epsilon_i(z)| \ll 1$. The equation of motion is linearized in this regime and becomes

$$i\partial_z \begin{pmatrix} \epsilon_1 \\ \epsilon_2 \end{pmatrix} = \begin{pmatrix} \mu + \eta\omega_{\mathrm{v}} & -\mu \\ \mu & -\eta\omega_{\mathrm{v}} - \mu \end{pmatrix} \begin{pmatrix} \epsilon_1 \\ \epsilon_2 \end{pmatrix}. \tag{4.20}$$
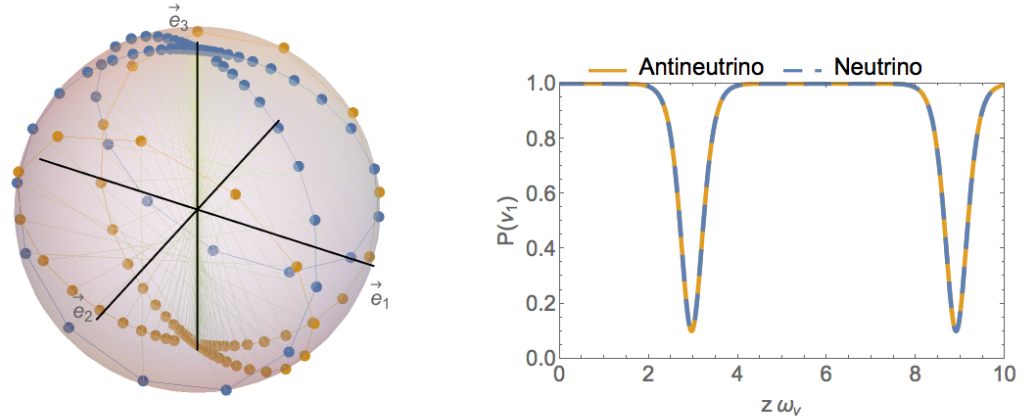
Figure 4.2: The numerical solution to the two-beam model. The left panel shows the position of the flavor isospin of the neutrino beam (in blue) and the antineutrino beam (in orange). The right panel shows the probabilities as functions of distance z (in unit of ω_v^{-1}) for the neutrinos and antineutrinos to remain in the $|\nu_1\rangle$ and $|\bar{\nu}_1\rangle$ states, which are the same as the survival probabilities of the electron flavor when mixing angle $\theta_v \ll 1$. In this calculation, the emission angles are $\theta_1 = 5\pi/6$ and $\theta_2 = \pi/6$, the neutrino self-interaction potential is $\mu = 5\omega_v$, and the neutrino mass hierarchy is inverted.

This equation has two normal modes with corresponds to the collective modes of neutrino oscillations:

$$\begin{pmatrix} \epsilon_1(z) \\ \epsilon_2(z) \end{pmatrix} = \begin{pmatrix} Q_{1\pm} \\ Q_{2\pm} \end{pmatrix} e^{iK_{z\pm}z}, \tag{4.21}$$

where $(Q_{1\pm}, Q_{2\pm})^{\mathrm{T}}$ are the eigenvectors of the two normal modes, and

$$K_{z\pm} = \pm\sqrt{\omega_v(\omega_v + 2\eta\mu)} \tag{4.22}$$

are the wavenumbers of the corresponding modes. For the normal mass hierarchy, $\eta = 1$, and $K_{z\pm}$ are always real. In this case, the electron flavor probability P_{ν_e} is always approximately 1. However, for the inverted neutrino mass hierarchy, $\eta = -1$, and $K_{z\pm}$ are imaginary when $\mu > \omega_v/2$. The normal mode with wavenumber $K_{z-} = -i\sqrt{\omega_v(2\mu - \omega_v)}$ is a runaway solution which explains the rapid decrease of P_{ν_e} in Fig. 4.2.

4.3 Dispersion Relations

In the two-beam model, I have assumed the neutrino flavor density matrix $\rho(z)$ depends on z only. For the neutrino medium in a real physical environment, $\rho(t, \mathbf{r})$ is a function of both time t and spatial coordinates $\mathbf{r}$. The collective mode a of neutrino oscillations takes the form

$$\epsilon_i(t, \mathbf{r}) = Q_i^{(a)} e^{\mathrm{i}(\Omega^{(a)}t - \mathbf{K}^{(a)} \cdot \mathbf{r})} \qquad (4.23)$$

where index i denotes the species and the propagation direction of the neutrino, and Ω_a and $\mathbf{K}_a$ are the oscillation frequency and wave vector of the corresponding collective mode, respectively. In this section, I will review the dispersion relations between Ω_a and $\mathbf{K}_a$ discussed by I. Izaguirre, G. Raffelt, and I. Tamborra in reference [37].

The equation of motion for the flavor transformation of a dense neutrino medium in flavor basis is

$$\mathrm{i}(\partial_t + \mathbf{v} \cdot \nabla)\rho = \left[\frac{\lambda}{2}\sigma_3 + \mathsf{H}_{\nu\nu}, \rho \right], \qquad (4.24)$$

where I have ignored the vacuum Hamiltonian. This is because the vacuum oscillation frequency of the neutrino

$$\omega_{\mathrm{v}} = \frac{\Delta m^2}{2E} \sim \frac{2\pi}{10\mathrm{km}} \left(\frac{\Delta m_{32}^2}{2.5 \times 10^{-3}\mathrm{eV}^2} \right) \left(\frac{10\mathrm{MeV}}{E} \right)$$
$$\sim \frac{2\pi}{330\mathrm{km}} \left(\frac{\Delta m_{12}^2}{7.5 \times 10^{-5}\mathrm{eV}^2} \right) \left(\frac{10\mathrm{MeV}}{E} \right)$$

is much smaller than the neutrino potential

$$\mu = \sqrt{2}G_{\mathrm{F}}n \sim \frac{1}{0.01\mathrm{km}} \left(\frac{100\mathrm{km}}{R} \right)^2 \left(\frac{1\mathrm{MeV}}{E} \right) \left(\frac{L}{10^{50}\mathrm{erg} \cdot \mathrm{s}^{-1}} \right),$$

where E is the typical energy of the supernova neutrino, n is the total number density of the neutrino, R is the distance from the center of the supernova, and L is the total luminosity of the neutrino. In Eqn. 4.24,

$$H_{\nu\nu} = \sqrt{2}G_{\mathrm{F}} \iint \mathrm{d}\Gamma' v^{\mu}v'_{\mu} \int \frac{E'^2 \mathrm{d}E'}{2\pi^2} \left((n'_{\nu_{\mathrm{e}}} - n'_{\nu_{\mathrm{x}}})\rho' - (n'_{\bar{\nu}_{\mathrm{e}}} - n'_{\bar{\nu}_{\mathrm{x}}})\bar{\rho}' \right), \qquad (4.25)$$

where

$$v^\mu = (1, \mathbf{v})^\mathrm{T} = (1, \sin\theta\cos\phi, \sin\theta\sin\phi, \cos\theta)^\mathrm{T} \tag{4.26}$$

is the four velocity of the neutrino, $\mathrm{d}\Gamma' = \frac{\mathrm{d}\cos\theta'\,\mathrm{d}\phi'}{4\pi}$ is the differential solid angle, and the primed quantities such as $\rho' = \rho_{\mathbf{v}'}(t, \mathbf{r})$ depend on the primed physical variable $\mathbf{v}'$. Without the vacuum Hamiltonian, the equation of motion for the antineutrino is the same as Eqn. 4.24.

In the supernova, the fluxes of non-electron-flavor neutrinos are approximately the same. It is convenient to define the electron lepton number (ELN) as [37],

$$G(\mathbf{v}) = \sqrt{2}G_\mathrm{F} \int \frac{E'^2 \mathrm{d}E'}{2\pi^2} (n_{\nu_\mathrm{e}}(\cos\theta', \phi', E') - n_{\bar{\nu}_\mathrm{e}}(\cos\theta', \phi', E')). \tag{4.27}$$

I will perform the linear stability analysis as in Sec. 4.2. For this purpose, I will assume the density matrices of the neutrinos and antineutrinos have the form

$$\rho_{\mathbf{v}}(t, \mathbf{r}) = \bar{\rho}_{\mathbf{v}}(t, \mathbf{r}) = \begin{pmatrix} 1 & \epsilon_{\mathbf{v}}(t, \mathbf{r}) \\ \epsilon_{\mathbf{v}}^*(t, \mathbf{r}) & 0 \end{pmatrix}, \tag{4.28}$$

where $|\epsilon| \ll 1$. Plugging this into the equation of motion, I obtain the linearized equation of motion

$$\mathrm{i}(\partial_t + \mathbf{v}\cdot\boldsymbol{\nabla})\epsilon = v^\mu\Phi_\mu\epsilon - \int \mathrm{d}\Gamma' v^\mu v'_\mu G(\mathbf{v})\epsilon', \tag{4.29}$$

where

$$\Phi_\mu = \left(-\int \mathrm{d}\Gamma' G(\mathbf{v}'), \int \mathrm{d}\Gamma' \mathbf{v}' G(\mathbf{v}')\right)^\mathrm{T}. \tag{4.30}$$

Assuming the solution in Eqn. 4.23, I obtain

$$v^\mu k_\mu Q_{\mathbf{v}} = -\int \mathrm{d}\Gamma' v^\mu v'_\mu G(\mathbf{v}')Q_{\mathbf{v}'}, \tag{4.31}$$

where

$$k_\mu = \begin{pmatrix} \omega \\ \mathbf{k} \end{pmatrix} = \begin{pmatrix} \Omega - \Phi_0 \\ \mathbf{K} - \boldsymbol{\Phi} \end{pmatrix}. \tag{4.32}$$

From Eqn. 4.31 I obtain the formal solution

$$Q_{\mathbf{v}} = -\frac{v^\mu a_\mu}{v^\alpha k_\alpha}, \tag{4.33}$$

where

$$a^\nu = \int d\Gamma G(\hat{\mathbf{v}}) v^\nu Q_{\mathbf{v}}. \tag{4.34}$$

Substituting Eqn. 4.33 into Eqn. 4.31, I obtain

$$v^\mu \Pi_\mu{}^\nu a_\nu = 0, \tag{4.35}$$

where

$$\Pi^\mu{}_\nu = \delta_\mu{}^\nu + \int d\Gamma G(\theta, \phi) \frac{v^\mu v_\nu}{\omega - k\hat{\mathbf{k}} \cdot \hat{\mathbf{v}}}. \tag{4.36}$$

The dispersion relation between ω and $\mathbf{k}$ is obtained by solving the characteristic equation [37]

$$\det\left(\Pi^\mu{}_\nu\right) = 0. \tag{4.37}$$

4.4 Flavor Instabilities and Dispersion-Relation Gaps

One can find the flavor instabilities of a neutrino medium by solving the dispersion relation (DR) between ω and $\mathbf{k}$ from Eqn. 4.37. A negative imaginary component of ω indicates a flavor instability in time, and a positive imaginary component of $\mathbf{k} \cdot \hat{\mathbf{z}}$ indicates a flavor instability in the $+z$ direction. I. Izaguirre et al. conjectured that the flavor instabilities exist in the gaps between the real branches of the dispersion relations [37]. In this section I will first explain this conjecture. Then I will show that this conjecture is actually incorrect.

4.4.1 Conjecture of the Relation between Flavor Instabilities and DR Gaps

I will consider a model with neutrinos emitted symmetrically about the z axis. For this model, the characteristic equation (4.37) reduces to

$$\det\left(\omega\mathsf{I} + \frac{1}{2}\begin{pmatrix} I_0 & 0 & 0 & -I_1 \\ 0 & -\frac{1}{2}(I_0 - I_2) & 0 & 0 \\ 0 & 0 & -\frac{1}{2}(I_0 - I_2) & 0 \\ I_1 & 0 & 0 & -I_2 \end{pmatrix}\right) = 0, \qquad (4.38)$$

where I is the rank-4 identity matrix and

$$I_m = \int_{-1}^{1} du\, G(u) \frac{u^m}{1 - u/v_{\mathrm{ph}}}. \qquad (4.39)$$

where $u = \cos\theta$, and $v_{\mathrm{ph}} = \omega/k$. Here I have assumed $\mathbf{k} = k\hat{\mathbf{z}}$. Eqn. 4.38 is satisfied if

$$\omega = -\frac{1}{4}\left(I_0 - I_2 \pm \sqrt{(I_0 + I_2 - 2I_1)(I_0 + I_2 + 2I_1)}\right) \qquad (4.40)$$

or

$$\omega = \frac{1}{4}(I_0 - I_2). \qquad (4.41)$$

I will call the solutions to Eqn. 4.40 the symmetric solutions (SS+ and SS− for the equations with the + and − signs) because they preserve the axial symmetry about the z axis. I will call the solutions to Eqn. 4.41 the asymmetric solutions (AS) because they break the axial symmetry.

To illustrate the conjecture by I. Izaguirre et al., I will consider the two-angle model where the neutrinos are emitted with two zenith angles θ_1 and θ_2. The ELN of the two-angle model is

$$G(u) = \mu \sum_{i=1,2} g_i \delta(u - u_i), \qquad (4.42)$$

where $\mu = \sqrt{2} G_{\mathrm{F}} n$ is proportional to the neutrino number density n, g_i are real numbers, and $u_i = \cos\theta_i$ ($i = 1, 2$). For any real k, the characteristic equations (4.40) and (4.41) are both quadratic equations of ω with two solutions. In Fig. 4.3 I

show the SS and AS of the dispersion relations $\omega(k)$ with $u_1 = -0.6$, $u_2 = 0.6$ and $g_1 = g_2 = 1$. In either case, both solutions $\omega(k)$ to the characteristic equations are real. However, there exist gaps between the DR curves $\omega(k)$ where there is no real solution $k(\omega)$ to the characteristic equations. Because the characteristic equations are also quadratic equations of k for any given real value of ω, a pair of complex solutions $k(\omega) = k_R(\omega) \pm ik_I(\omega)$ exist in the DR gap of ω (see Fig. 4.3).

The observation of the result of the two-angle model leads I. Izaguirre et al. to conjecture that the flavor instabilities are associated with the DR gaps. They also studied the dispersion relations using a continuous ELN distribution from a 1D supernova simulation[1] which are reproduced in Fig. 4.4.
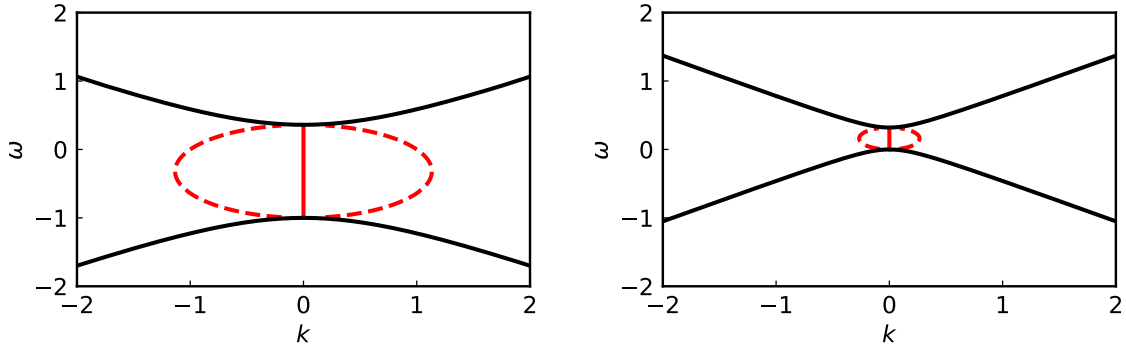
Figure 4.3: The SS (left) and AS (right) of the dispersion relations for the two-angle model. The thick black curves represent $\omega(k)$ for real k. The red dashed and thin solid curves are $k_R(\omega)$ and $k_R(\omega) \pm k_I(\omega)$ for real ω within the DR gap of ω. Both ω and k are measured in terms of the neutrino potential μ.

4.4.2 Refutation of the Conjecture

The association of the flavor instability in space, i.e., $k_I(\omega) \neq 0$, with a DR gap in ω seems fortituous for the two-angle model. As I explained previously, for the two-angle model, the characteristic equations are quadratic equation of k for any given ω. Therefore there always exists a pair of complex solutions between the DR

---

[1]The data is from the Garching Core-Collapse Supernova Archive at `http://wwwmpa.mpa-garching.mpg.de/ccsnarchive/archive.html`
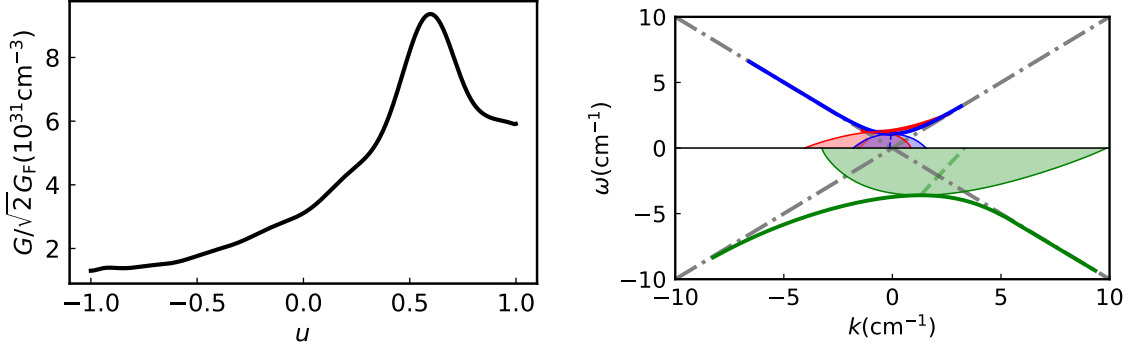
Figure 4.4: The SS+ (green), SS− (blue) and AS (red) of the dispersion relations (right panel) for a net electron flavor neutrino density distribution $n_{\nu_e}(u) - n_{\bar\nu_e}(u)$ obtained from a Garching 1D supernova simulation (left panel). The thick solid curves represent the dispersion relations when both ω and k are real. The dashed curves represent $k_R(\omega)$ in the DR gap of ω, and the thin solid curves (bouding the shaded regions) are $k_R(\omega) \pm k_I(\omega)$.

gap in ω. This is not the case when the neutrinos are emitted with more than two zenith angles.

In Fig. 4.5, I show the dispersion relations of a three-angle model with ELN

$$G(u) = 0.5\mu\delta(u + 0.1) + \mu\delta(u - 0.4) + \mu\delta(u - 0.6). \tag{4.43}$$

For this model, there exist complex solutions of $k(\omega)$ even though there is no DR gap in ω. This is because the characteristic equations are cubic equations of k for given ω which admit three solutions. In certain ranges of ω there is only one real solution of $k(\omega)$. The other two solutions must be complex which indicates flavor instablities in space.

The conjecture between the flavor instablities and DR gaps does not work for the models with continuous ELN distribution $G(u)$ either. In Fig. 4.6 I show the dispersion relations for a step-like distribution

$$G(u) = \begin{cases} -0.1 & \text{if } -1 < u < -0.3, \\ 1 & \text{otherwise.} \end{cases} \tag{4.44}$$

One sees that, for this model, the SS+ and SS− solutions merge into a continuous DR curve so that there is no gap in ω. However, there do exist complex solutions
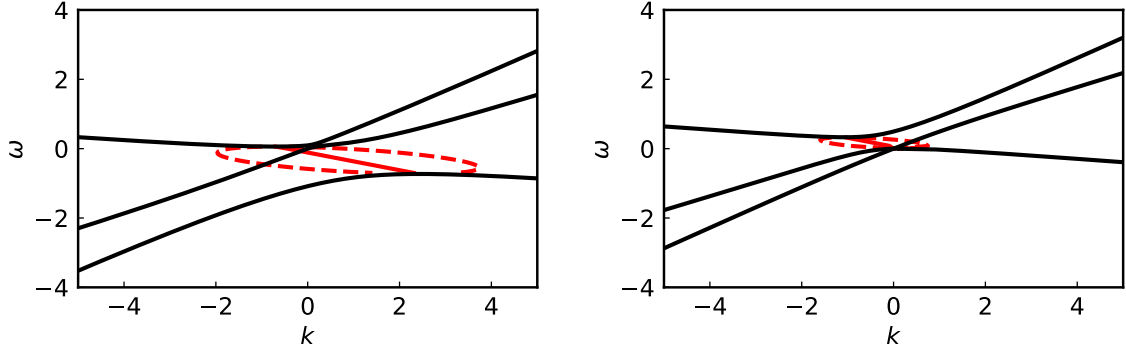
Figure 4.5: The same as Fig. 4.3 but for the three-angle model described in the text.
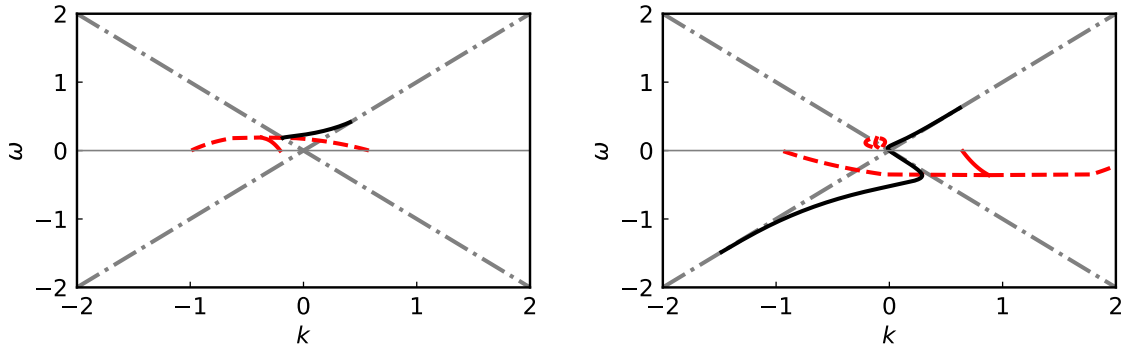
Figure 4.6: The same as Fig. 4.3 but for the ELN distribution in Eqn. 4.44.

$k(\omega)$ for certain values of ω.

As shown in Fig. 4.4 and Fig. 4.6, AS dispersion relations $k(\omega)$ appear only in the region where $\omega > 0$. This can be proved analytically as follows. Suppose there exist dispersion relations $k(\omega) = k_{\mathrm{R}}(\omega) + k_{\mathrm{I}}(\omega)$ for $\omega \to 0$. Using Sokhotski–Plemelj theorem, I can rewrite the characteristic equation

$$k = \frac{1}{4} \int \mathrm{d}u G(u) \frac{1 - u^2}{\omega/k - u}. \tag{4.45}$$

as

$$k_{\mathrm{R}} = \frac{1}{4} \left(\mathcal{P} \int \mathrm{d}u G(u) \frac{1 - u^2}{-u} \right) \tag{4.46a}$$

$$k_{\mathrm{I}} = \frac{\pi}{4} G(0) \, \mathrm{Sign}\,(\omega) \, \mathrm{Sign}\,(k_{\mathrm{I}}) , \tag{4.46b}$$

where $\mathcal{P}$ denotes the principal value of the integral. As long as $G(0) \neq 0$, ω must have the same sign as $G(0)$ which implies that $k(\omega)$ exists only on one side of the

vicinity of $\omega = 0$. For the two scenarios depicted in Fig. 4.4 and Fig. 4.6, $G(0) > 0$ and $k(\omega)$ exist only in the upper half plane of ω. This shows that, at least near $\omega = 0$, the abscence of a DR $\omega(k)$, i.e., a "gap" in ω, is not always associated with the flavor instabilities in space.

Eqn. 4.46 can be used to determine the values of k_R and k_I in the limit of $\omega \to 0$ for the AS branch of the dispersion relations. One can apply the same method to the SS branches which gives

$$(4k_R - J_{-1} + J_1)^2 - (\mathrm{Sign}(\omega k_I)\pi G(0) + 4k_I)^2 \tag{4.47}$$

$$= -(J_{-1} + J_1)\,\pi\,\mathrm{Sign}(\omega k_I)G(0) \tag{4.48}$$

and

$$k_I = -\frac{\pi}{4}G(0)\,\mathrm{Sign}(\omega k_I)\left(1 \pm \frac{J_{-1} + J_1}{4k_R - J_{-1} + J_1}\right), \tag{4.49}$$

where

$$J_n = \mathcal{P}\int G(u)u^n \mathrm{d}u, \tag{4.50}$$

and the $+$ and $-$ signs are for SS+ and SS−, respectively. Eqn. 4.48 and Eqn. 4.49 show that $k(\omega)$ exist on both sides of the vicinity of $\omega = 0$ but may be different for SS+ and SS−.

4.5 Neutrino Halo Problem

Cherry et al showed that neutrino flavor conversions are greatly affected by the back scattered neutrinos in supernovae, which is called the neutrino halo problem [24]. Neutrinos around supernovae are scattered and some of them are scattered to move almost backward. On the other hand, neutrino self-interactions is proportional to the inner product of momenta of neutrinos, which leads to the dependence on $1 - \cos\theta$ where θ is the angles between momenta of two neutrinos. Most of the research has been concentrating on mostly forward scattering, with small values for $1 - \cos\theta$. For backward scattered neutrinos, the interaction potential can be much larger than the forward scattered neutrino potential. Though the work by S. Sarikas et al showed

that matter suppression is still significant within this region [26], it is not clear how exactly the neutrino halo alters neutrino oscillations. The halo problem itself is worth more calculations. In this chapter, I will present a relaxation method for this problem. The focus will be on the numerical method itself.

4.5.1   Line Model

I will use the line model to build intuitions of the halo problem. The halo problem is simplified to have neutrinos emitted from a line $z = 0$ homogeneously, which are reflected from a certain distance $z = L$. In general, the reflection angles doesn't have to be Snell's law. The scattering can be in any angle with different amplitudes. Here I am using this very simple Snell's law just to explore the effect of halo. In summary, I use the following assumptions.

- Neutrinos are emitted from a line, which is not the case in a real supernova.

- Neutrinos are emitted with translation symmetry on the line. Breaking the symmetry might bring in other qualitatively different results.

- Neutrinos are reflected from a certain surface $z = L$, which is different from reality where neutrinos are scattered everywhere.

- Neutrinos are reflected according to Snell's law.

- Neutrinos are homogeneously reflected at $z = L$.

Fig. 4.7 describes the above model in details. The state of the left-going beam and right-going beam are denoted as ρ_1 and ρ_2, respectively. Each beam has self-interaction potential n_i.

4.5.2   Neutrino Beams Only

As a first step, I calculated the neutrino oscillations with neutrino beams only and propagating with $\theta_1 = \theta_2 = \pi/2$ (see Fig. 4.8) Before I rush to the numerical results,
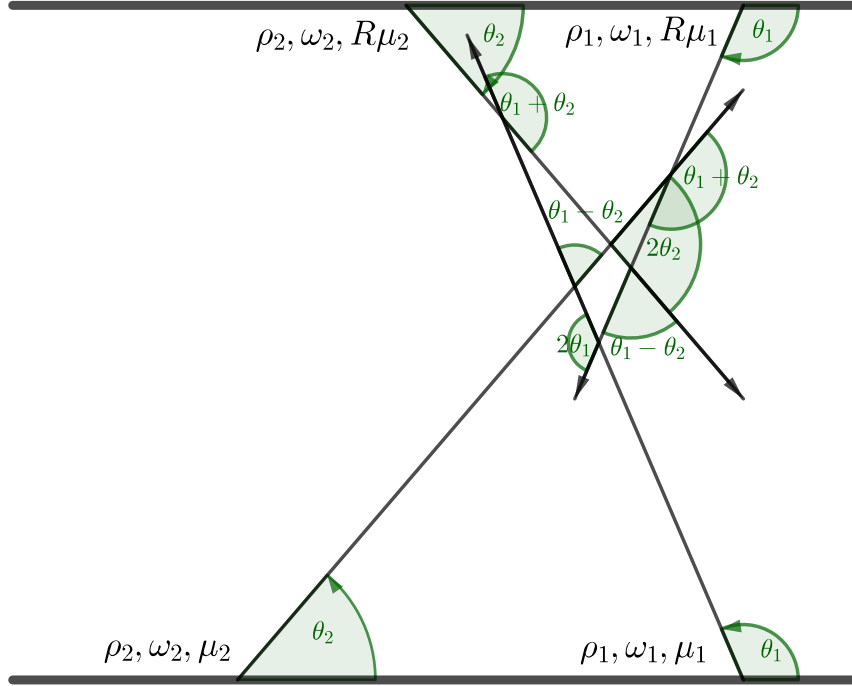
Figure 4.7: A general line model for halo problem. The neutrinos are emitted from the bottom line and reflected at the top line. Two neutrino beams are demonstrated in the figure. The beams are reflected from a surface at $z = L$.

I will linearize the equation of motion and work out the linear stability analysis for this simplified line model.

In the linear regime, I define the density matrices for forward and backward beams to be

$$\rho_F = \frac{1}{2} \begin{pmatrix} 1 & \epsilon_F \\ \epsilon_B^* & -1 \end{pmatrix}$$

$$\rho_B = \frac{1}{2} \begin{pmatrix} 1 & \epsilon_B \\ \epsilon_B^* & -1 \end{pmatrix}.$$
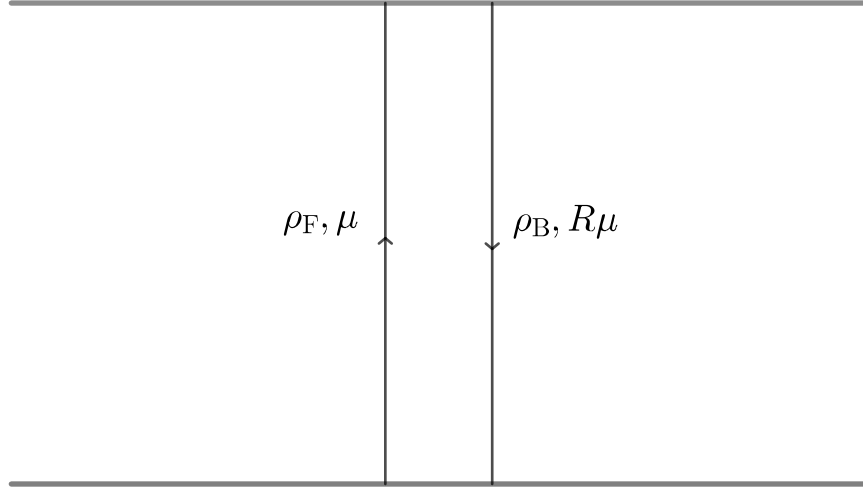
Figure 4.8: The simplified line model similar to Fig. 4.7 but with neutrino beams only and $\theta_1 = \theta_2 = \pi/2$.

The Hamiltonian for forward and back ward beams are

$$H_F = H_v + R\mu\rho_B$$

$$H_B = H_v + \mu\rho_F.$$

I will investigate the instability for zero mixing angle for new instabilities. The linearized equation of motion can be simplified to

$$i\partial_z \begin{pmatrix} \epsilon_F \\ \epsilon_B \end{pmatrix} = \begin{pmatrix} -\omega_v + R\xi\mu & -R\xi\mu \\ \xi\mu & \omega_v - \xi\mu \end{pmatrix} \begin{pmatrix} \epsilon_F \\ \epsilon_B \end{pmatrix}.$$

This equation can be easily solved. The eigenvalues are

$$\Omega_+ = \frac{1}{2}((R-1)\xi\mu + \sqrt{\Delta})$$
$$\Omega_- = \frac{1}{2}((R-1)\xi\mu - \sqrt{\Delta}),$$

where

$$\Delta = (1-R)^2\mu^2\xi^2 - 4\mu\xi\omega_v(1+R) + 4\omega_v^2. \tag{4.51}$$

The corresponding eigenvectors are

$$V_+ = \begin{pmatrix} \frac{-2\omega_v + \xi\mu(1+R) + \sqrt{\Delta}}{2\xi\mu} \\ 1 \end{pmatrix}$$

$$V_- = \begin{pmatrix} \frac{-2\omega_v + \xi\mu(1+R) - \sqrt{\Delta}}{2\xi\mu} \\ 1 \end{pmatrix}.$$

The general solution to the equation is

$$\begin{pmatrix} \epsilon_F(z) \\ \epsilon_B(z) \end{pmatrix} = C_+ V_+ e^{-i\Omega_+ z} + C_- V_- e^{-i\Omega_- z}.$$

The special property about this reflection problem is that the density matrices for the forward and backward beams should be the same at the reflection point, say $z = L$. With such a simple relation, we can find the relations between $C_\pm$ by setting $\epsilon_F(L) = \epsilon_B(L)$,

$$\frac{C_+}{C_-} = e^{-i(\Omega_- - \Omega_+)L} \frac{\sqrt{\Delta} + 2\omega_v + \mu\xi(1-R)}{\sqrt{\Delta} - 2\omega_v - \mu\xi(1-R)}. \tag{4.52}$$

The solution to be problem can be simplified,

$$\begin{pmatrix} \epsilon_F(z) \\ \epsilon_B(z) \end{pmatrix} = C_- e^{-i\Omega_- L} \left(\frac{\sqrt{\Delta} + 2\omega_v + \mu\xi(1-R)}{\sqrt{\Delta} - 2\omega_v - \mu\xi(1-R)} V_+ e^{-i\Omega_+(z-L)} + V_- e^{-i\Omega_-(z-L)} \right). \tag{4.53}$$

I am interested in the absolute values of each elements so that the overall factors can be neglected. The forward beam evolution is obtained by taking the absolute value of ϵ_F,

$$|\epsilon_F| \propto |(2\omega_v + \xi\mu(1-R) + i\delta)(-2\omega_v + \xi\mu(1+R) + i\delta)e^{\delta(z-L)}$$
$$+ (-2\omega_v - \xi\mu(1-R) + i\delta)(-2\omega_v + \xi\mu(1+R) - i\delta)e^{-\delta(z-L)}|,$$

in which $\sqrt{\Delta}$ is replaced by $i\delta$. I collect terms and verify that it has the form

$$|\epsilon_F| \propto A + B\cosh(2\delta(L-z)), \tag{4.54}$$

where $B \leq 0$. The only z dependent term is $\cosh(2\delta(L-z))$, which is decreasing within $[0, L]$ and is increasing in $[L, 2L]$. The slope at $z = L$ is 0. An example is plotted in Fig. 4.9.
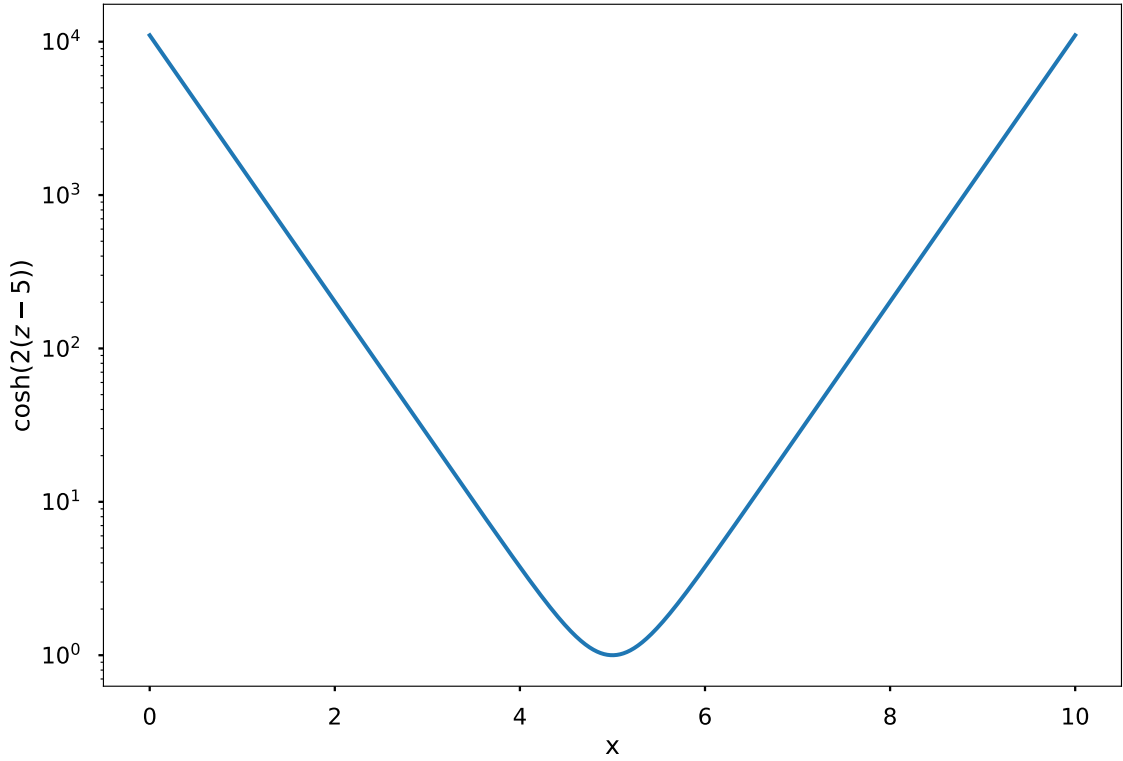
Figure 4.9: An example of $\cosh(2\delta(z-L))$ with $\delta = 1$, and $L = 5$. This function always reach the minimum at $z = L$.

We expect the numerical calculations bare the same behavior that the instability leads to no growth but decrease in flavor conversion, assuming the neutrinos start from electron flavor. The result indeed confirms it. Fig. 4.10 is an example of it.

I use the relaxation method to solve this simplified halo problem. The algorithm is meant to find the equilibrium state of neutrino oscillations with the presence of halo.

1. Calculate forward beam using 0 backward beam;

2. Calculate backward beam using forward beam calculated in 1;

3. Calculate forward beam using backward beam calculated in 2;

4. Repeat until the beams reach equilibrium.
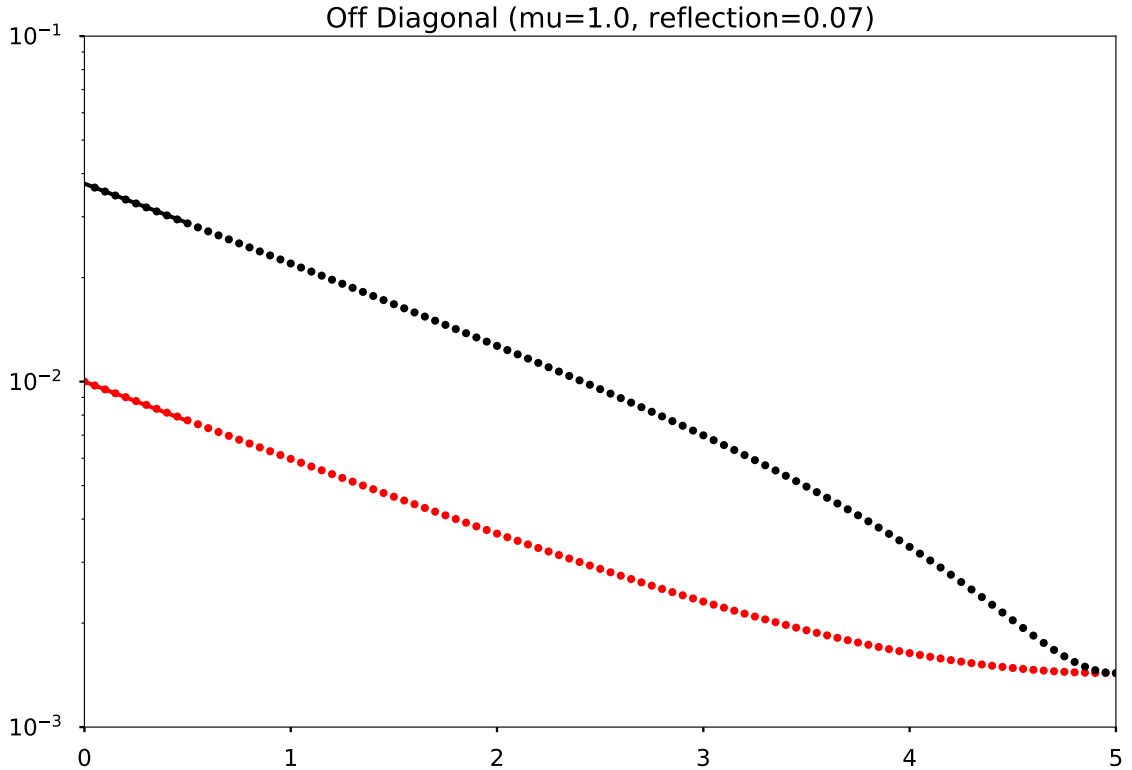
Figure 4.10: Absolute value of off diagonal element for $\mu = 1.0$, $R = 0.07$, $L = 5$, with normal hierarchy. The red dots are for the forward beam and the black dots are for the backward beams. The lines are indicating the predictions of linear stability analysis.

For linear stability analysis, I usually identify real characteristic values of the linearized equation of motion. In bipolar model as explained in Sec. B.3, real characteristic values of the equation of motion indicates exponential growth, while it always indicates exponential decrease in this simplified halo problem.

I expect that only normal hierarchy has an instability region which is trivial since I noticed that the backward beam is acting like antineutrino beams but with different

hierarchies.

$$i\partial_t \mathbf{s}_F = \mathbf{s}_F \times (\mathbf{H}_v + R\mu\mathbf{s}_B) \tag{4.55}$$

$$i\partial_t \mathbf{s}_B = \mathbf{s}_B \times (-\mathbf{H}_v - \mu\mathbf{s}_F). \tag{4.56}$$

Compare to Eq. B.25, I notice that the reflected beam works as an antineutrino beam but the system becomes the opposite hierarchy compared to bipolar model. I find the instability regions in Fig. 4.11.
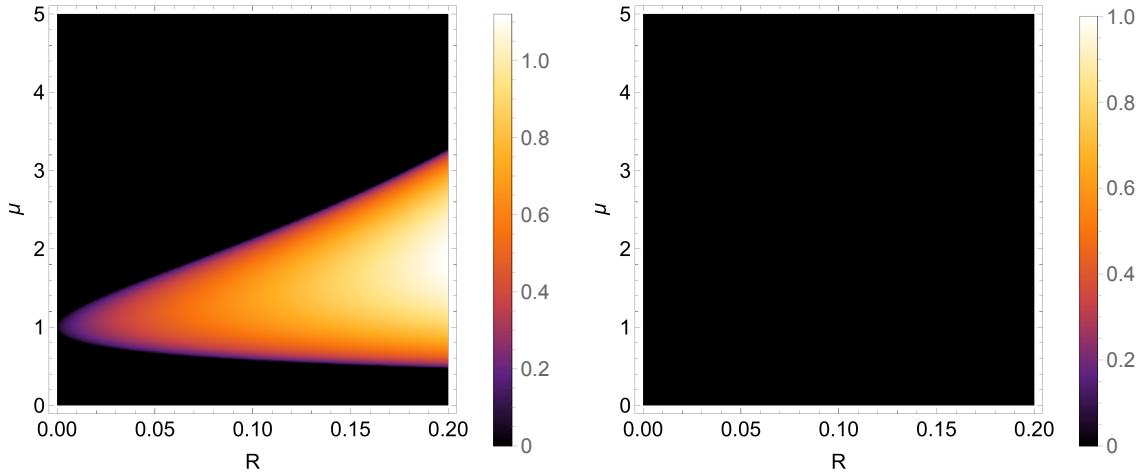
Figure 4.11: Instability regions for normal hierarchy (left) and inverted hierarchy (right) as a function of neutrino potential μ and reflection coefficient R, with vacuum mixing angle set to 0. No instabilities is found in inverted hierarchy.

4.5.3   Two Beams Model with Reflection

The model is naturally extended to a two beams model including both neutrinos and antineutrinos. The configuration is exactly the same as shown in Fig. 4.7.

As the first step we work out the linear stability analysis. The four equations of

motion are

$$i\partial_z\rho_1 = [H_1, \rho_1], \tag{4.57}$$

$$i\partial_z\rho_2 = [H_2, \rho_2], \tag{4.58}$$

$$-i\partial_z\rho_3 = [H_3, \rho_3], \tag{4.59}$$

$$-i\partial_z\rho_4 = [H_4, \rho_4], \tag{4.60}$$

where $_1$ and $_2$ are the quantities for two forward beams while $_3$ and $_4$ are the quantities for the corresponding backward going beams. For the purpose of this analysis we set $\theta_v = 0$. The Hamiltonians are

$$H_1 = -\eta\omega_v\sigma_3 + g_2\chi_-\mu_2\rho_2 + g_2\chi_+R\mu_2\rho_4 + g_1\chi_1R\mu_1\rho_3, \tag{4.61}$$

$$H_2 = \eta\omega_v\sigma_3 + g_1\chi_-\mu_1\rho_1 + g_2\chi_2R\mu_2\rho_4 + g_1\chi_+R\mu_1\rho_3, \tag{4.62}$$

$$H_3 = -\eta\omega_v\sigma_3 + Rg_2\chi_-\mu_2\rho_4 + g_2\chi_+\mu_2\rho_2 + g_1\chi_1\mu_1\rho_1, \tag{4.63}$$

$$H_4 = \eta\omega_v\sigma_3 + Rg_1\mu_1\chi_-\rho_3 + g_1\chi_+\mu_1\rho_1 + g_2\chi_2\mu_2\rho_2. \tag{4.64}$$

I have defined

$$\chi_+ = 1 - \cos(\theta_1 + \theta_2),$$

$$\chi_- = 1 - \cos(\theta_1 - \theta_2),$$

$$\chi_1 = 1 - \cos(2\theta_1),$$

$$\chi_2 = 1 - \cos(2\theta_2),$$

and g_i represents the energy spectrum of the neutrinos and η stands for the hierarchy.

4.6   Relaxation Method for Neutrino Halo Problem

We choose a relaxation method scheme to solve this non-local boundary value problem numerically. To begin with, we write down the discretization scheme.

$$\rho(t + \Delta t) = [\cos(2h\Delta t)\rho_n - 2u_i\rho_i u_n]\,\sigma_n \tag{4.65}$$

$$= \left[\cos(2h\Delta t)\rho_n + 2\sin^2(h\Delta t)u_i'\rho_i u_n'\right]\sigma_n \tag{4.66}$$

The reason that we use fixed step size for this problem is that it's easier to calculate the neutrino self-interactions on such fixed grids. The algorithm is described as

1. Calculate forward beam using 0 backward beam;

2. Calculate backward beam and forward beam together using the state of beams from the previous step current counter beams;

3. Repeat the previous step until the state of the beams reach equilibrium.

To speed up the calculations, I also implemented OpenMP for parallel computing. The code is tested using vacuum oscillations (shown in Fig. 4.12) and bipolar models. The reason that we still have conversions is because of the vacuum term, which is additional to linear stability analysis (see Fig. 4.13). I also proved that the neutrino oscillations reached equilibrium quickly as shown in Fig. 4.14 where the neutrino flavors are indicated by colors.
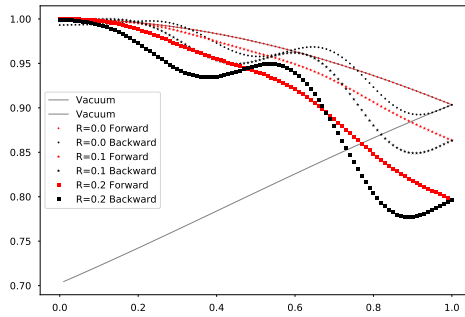
Figure 4.12: The validation of the code by setting reflection to zero and approach vacuum for single forward beam. For nonzero reflections, more conversion is done, which makes sense due to the similarity between R and the asymmetry parameter α in bipolar model.

4.7 Conclusion

The dispersion relations can be extracted from the linearized form of the equation of motion for collective neutrino oscillations. The dispersion relation becomes quadratic
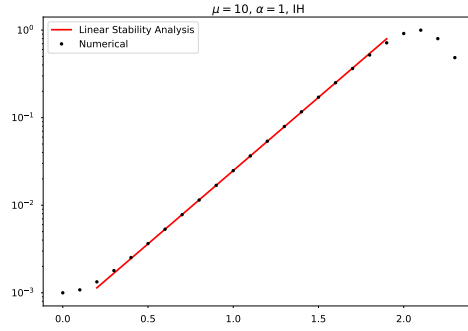
Figure 4.13: The validation of the code by setting reflection to zero and compare with bipolar model for two beams case, where the slope is matching the theoretical value 3.85.
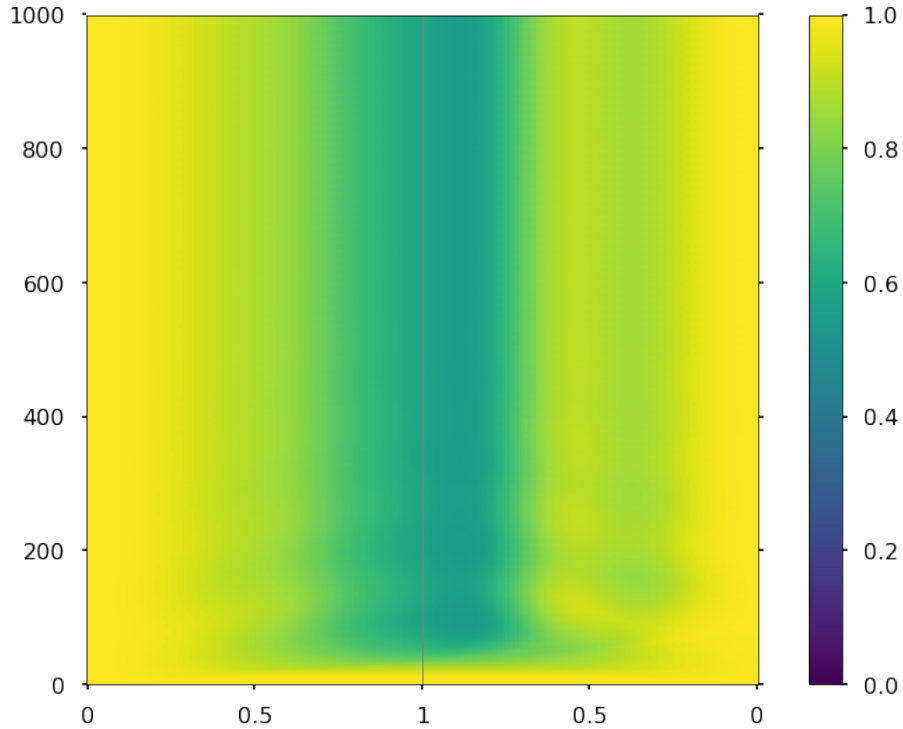
Figure 4.14: Relaxation method reaches equilibrium after some steps. The horizontal axis is the z direction while the vertical axis is the number of iteration steps. The color indicates the survival probability for electron flavor. This calculation sets $\mu = 4$, $R = 0.2$, and is done within range $[0, 1]$. Equilibrium is reached around step 400 and the neutrino states stays in equilibrium.

for neutrino emission with two zenith angles. Thus two solutions should be found for ω and k. The dispersion relations are hyperbolas and the gaps between the lines corresponds to instabilities. However, this correspondence doesn't hold for neutrinos emitted from more zenith angles. For more realistic spectrum, I have proved that instabilities propagate in regions of either $\omega > 0$ or $\omega < 0$ and never cross $\omega = 0$. Hence the dispersion relation gaps should be defined as gaps between the dispersion relation curves and the axis $\omega = 0$ instead of the dispersion relation curves. I have also showed that instabilities is not necessarily shown as gap in dispersion relations for neutrino emission with more than two zenith angles and box spectrum with crossing. Through the discussions, I demonstrated that the relation between dispersion relation gaps and instabilities should be used with caution.

The second problem discussed in this chapter is the halo problem, which brings in more complexities to the neutrino oscillations. In the spirit of numerical methods, I developed a parallelable relaxation method, using C++ and OpenMP. Both the analytical and numerical results showed that for the two realms, either single forward beam or two forward beams, the results are compared with bipolar model. This simple model is very similar to the bipolar model thus I can perform linear stability analysis and verify my numerical method. The reflection indeed may enhance the flavor conversions but it is not a new type of instability. Future work should be done to explore the effect of symmetry breaking and multiple emission beams.

Chapter 5

Conclusion

The neutrino is a common product in astrophysical environments which makes neutrino physics a key ingredient of astrophysics. Since different neutrino flavors have different impact on the dynamics of astrophysical objects, identifying the flavor dynamics of the neutrino becomes important. One the other hand, the neutrino converts between different flavors while it propagates due to the mismatch of flavor states and mass states. Thus the neutrino doesn't maintain its flavor as produced. Even more, the conversions are altered by neutrino interactions with the matter or the neutrino itself.

The interactions with matter lead to the so called MSW effect where neutrinos may experience maximum flavor conversion for some specific matter density. In this dissertation, I have also explained the neutrino parametric oscillations where the varying matter profile serves as the driving field for the neutrino two-level quantum system. The matter profile drives the neutrino oscillations to resonance when the frequency of the driving potential matches the energy gap of the two energy levels, which is quite similar to Rabi oscillations. However, the matter potential provides more than one driving frequencies. Those different driving frequencies interfere with each other, which indicates that a second driving potential might lead to destruction of resonances of the original driving potential. This has been proved in the dissertation. I also prove that the interference might also enhance the resonance. The Rabi

oscillations point of view has provided a simple picture to understand the neutrino oscillations in oscillatory matter profile.

For future research, neutrino oscillations in more realistic matter profile has to be calculated to locate the possible resonances. For example, the matter density in supernovae is Kolmogorov-like. To understand the matter effect on neutrino oscillations in supernovae, the possible resonances can be identified using the resonance condition and the interference effect. As for applications of this parametric resonance, one of them is neutrino tomography. Using resonances of neutrino oscillations at different energies, it is possible to infer the interior structure of celestial objects.

As for neutrino oscillations with self-interactions, the equation of motion can be linearized for linear stability analysis in this dissertation. Linear stability analysis is a very useful tool for neutrino oscillations in dense neutrino media. It reveals whether the neutrino will be converted to other flavors. While linear stability analysis has been used frequently in the research, I. Izaguirre et al. has concluded in [37] that the dispersion relations of neutrino oscillations can be defined and they correspond to flavor instabilities. The idea may sound pretty but I showed in this dissertation that dispersion relations gaps and flavor instabilities are not simply related. Flavor instabilities do not always exist within gaps of dispersion relations. They exist even when no gaps are found in the dispersion relations.

Recently, F. Capozzi has developed more theories to use the dispersion relations to understand flavor instabilities [36]. They have found criteria for four different types of instabilities. The two important instabilities are absolute flavor instability and convective flavor instability, where the neutrino flavor perturbation grows everywhere and the neutrino flavor perturbation decays locally but grows in other locations, respectively. However, the theories has to be verified for multiple emission angles.

The so called neutrino halo problem is also discussed in this dissertation. The problem arises since the supernova neutrinos are scattered when they are propagating. The backward propagating neutrinos encounters the forward propagating neutrinos and interact with them. The problem becomes mathematically and nu-

merically difficult since it is a nonlocal boundary value problem. In this dissertation, I have designed and tested the relaxation method to solve the halo problem numerically. The relaxation method starts with some initial configuration of neutrino states in space and allow the neutrinos to relax to an equilibrium configuration. To efficiently solve the problem, the code utilizes the power of parallel computing. I also found that the single beam line model, where neutrinos are emitted on a line all in one direction and reflected at the same distance, has similar dynamics as the bipolar model. This similarity makes it possible to solve the linear regime of the problem and validate the numerical.

The neutrino halo problem brings in a lot of variables to the neutrino oscillations around supernovae. Since the relaxation method has been proven to work, more variable models can be solved numerically and understand the effect of the neutrino halo. The symmetries in the halo problem should be broken to investigate the possible new flavor instabilities.

Appendices

Appendix A

Conventions

A.1 Notations

- Variables with sans-serif fonts are matrices.

- Variables in bold are vectors in space-time.

- Variables with arrows are vectors in flavor-isospin space.

A.2 Terms

- Normal hierarchy for two-flavor scenario is always defined as $m_2^2 - m_1^2 > 0$, i.e., $\omega_{\mathrm{v}} > 0$.

- Inverted hierarchy for two-flavor scenario is defined as $m_2^2 - m_1^2 < 0$, i.e., $\omega_{\mathrm{v}} < 0$.

- Solar neutrino mass splitting is δm_{12}, while atmospheric neutrino mass splitting refers to δm_{23}.

A.3 Units

Natural units system makes the calculations of neutrinos convenient. By definition, we set reduced Planck constant and speed of light to be 1, $\hbar = 1 = c$. The conversion between natural units and SI can be down by using the following relations,

$$1\text{GeV} = 5.08 \times 10^{15}\text{m}^{-1} \tag{A.1}$$

$$1\text{GeV} = 1.8 \times 10^{-27}\text{kg} \tag{A.2}$$

To convert between different physical quantities in this thesis, I always use the following tips.

- The energy-mass-momentum relations becomes $E^2 = p^2 + m^2c^2 = p^2 + m^2$. Thus mass m, momentum $\mathbf{p}$ and energy E have the same dimension.

- An example of angular momentum in quantum mechanics is $L_z = m\hbar = m$ where m is a quantum number. $\hbar$ is of dimension angular momentum.

- A plane wave in quantum mechanics is $\Psi = Ae^{\frac{Et-px}{\hbar}}$. $\frac{Et-px}{\hbar}$ should be dimensionless, which means px has dimension angular momentum, which is obvious, meanwhile we notice that Et also has the dimension of angular momentum. Previously we noticed momentum has the same dimension with energy, we should have time t with the same dimension of length x. Also we can conclude that length and time have the same dimension as $1/E$.

A.4 Pauli Matrices and Rotations

Given a rotation

$$U = \begin{pmatrix} \cos\theta & \sin\theta \\ -\sin\theta & \cos\theta \end{pmatrix}, \tag{A.3}$$

its effect on Pauli matrices are

$$U^\dagger \sigma_3 U = \cos 2\theta\sigma_3 + \sin 2\theta\sigma_1 \tag{A.4}$$

$$U^\dagger \sigma_1 U = -\sin 2\theta\sigma_3 + \cos 2\theta\sigma_1. \tag{A.5}$$

A.5 Lorentzian Distribution

Three-parameter Lorentzian function is

$$f_{x_0,\sigma,A}(x) = \frac{1}{\pi} \frac{\sigma}{\sigma^2 + (x - x_0)^2}, \tag{A.6}$$

which has a width 2γ.

A.6 Fourier Series

The convention for the Fourier series used in this thesis is

$$\lambda(x) = \sum_{n=-\infty}^{\infty} \Lambda_n \exp\left(\frac{i2\pi nx}{X}\right) = \sum_{n=-\infty}^{\infty} \Lambda_n \exp\left(i\omega_0 nx\right), \tag{A.7}$$

where $\omega_0 = \frac{2\pi}{X}$. The coefficients are evaluated using the orthogonal relation of exponential functions for $n \neq 0$,

$$\Lambda_n = \frac{1}{X} \int_0^X \lambda(x)e^{-i\omega_0 nx}dx \tag{A.8}$$

$$= \frac{1}{X} \left(\int_0^{X_1} \lambda_1 e^{-i\omega_0 nx}dx + \int_{X_1}^{X_1+X_2} \lambda_2 e^{-i\omega_0 nx}dx \right) \tag{A.9}$$

$$= \frac{1}{X} \frac{X}{-i2\pi n} \left(\lambda_1 e^{-i\omega_0 nX_1} + \lambda_2 \left(e^{-i\omega_0 nX} - e^{-i\omega_0 nX_1} \right) \right) \tag{A.10}$$

$$= \frac{i}{2\pi n} \left(-\lambda_1 + (\lambda_1 - \lambda_2)e^{-i2\pi nX_1/X} + \lambda_2 e^{-i2\pi n} \right). \tag{A.11}$$

For $n = 0$, we have

$$\Lambda_0 = \frac{X_1\lambda_1 + X_2\lambda_2}{X}. \tag{A.12}$$

For functions with specific parity, the Fourier series is much more simpler. I'll list below the Fourier series for even functions, since no odd functions are used in this thesis. In general the Fourier series of a periodic function defined on $\left[-\frac{X}{2}, \frac{X}{2}\right]$ is

$$\lambda(x) = \frac{a_0}{2} + \sum_{n=1}^{\infty} a_n \cos(n2\pi x/X) + \sum_{n=1}^{\infty} b_n \sin(n2\pi x/X), \tag{A.13}$$
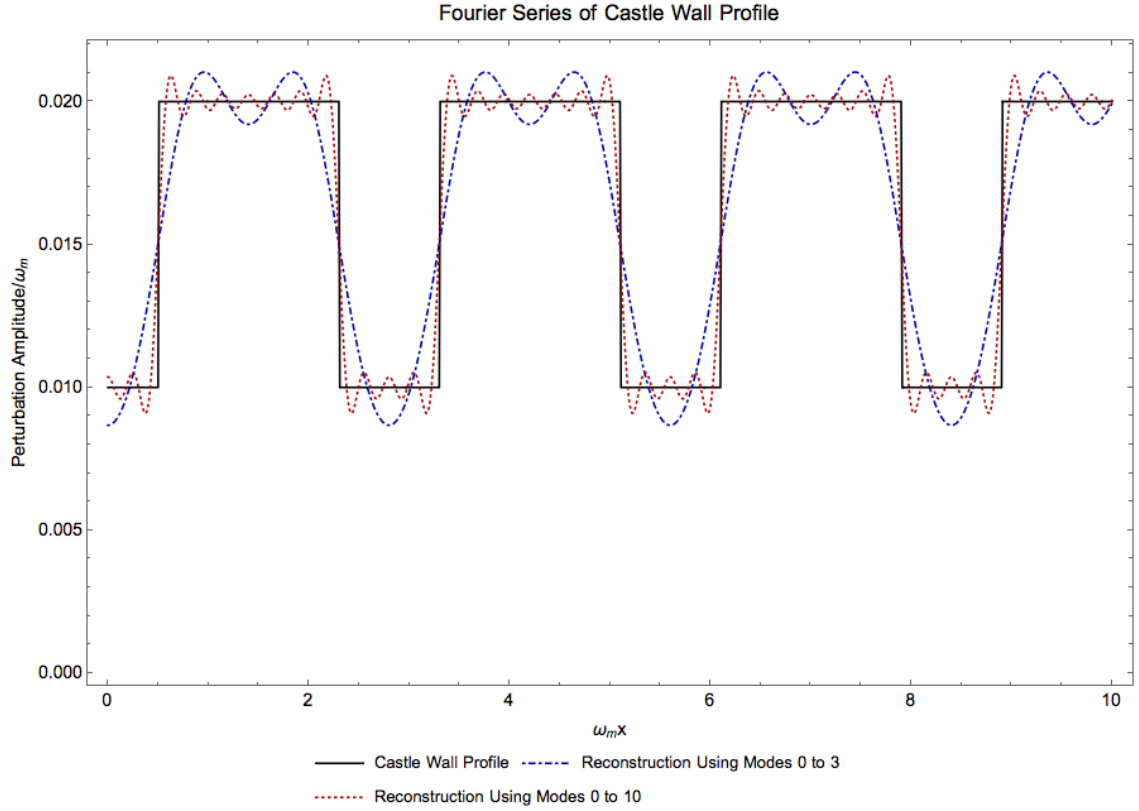
Figure A.1: Approaching an even function with Fourier series. The blue dash dotted line is the reconstruction of castle wall profile using 0 to 3 Fourier modes. The red dotted line is the reconstruction using 0 to 10 Fourier modes.

where

$$a_0 = \frac{2}{X} \int_{-X/2}^{X/2} \lambda(x) dx \tag{A.14}$$

$$a_n = \frac{2}{X} \int_{-X/2}^{X/2} \lambda(x) \cos(n2\pi x/X) dx \tag{A.15}$$

$$b_n = \frac{2}{X} \int_{-X/2}^{X/2} \lambda(x) \sin(n2\pi x/X) dx. \tag{A.16}$$

For even function $\lambda(x)$, we have

$$\lambda(x) = \frac{1}{2}a_0 + \sum_{n=1}^{\infty} a_n \cos(n2\pi x/X). \tag{A.17}$$

We shift the castle wall profile and make it always even, as shown in Fig. A.1, so

that

$$\lambda(x) = \begin{cases} \lambda_2, & -\frac{X_2}{2} - \frac{X_1}{2} \leq x \leq -\frac{X_1}{2} \\ \lambda_1, & -\frac{X_1}{2} \leq x \leq \frac{X_1}{2} \\ \lambda_2, & \frac{X_1}{2} \leq x \leq \frac{X_1}{2} + \frac{X_2}{2} \end{cases} \tag{A.18}$$

Fourier series of the profile is

$$\lambda(x) = \frac{1}{2}\Lambda_0 + \sum_{q=1}^{\infty} \Lambda_q \cos\left(\frac{2\pi q x}{X}\right) = \frac{1}{2}\Lambda_0 + \sum_{q=1}^{\infty} \Lambda_q \cos\left(\omega_0 q x\right), \tag{A.19}$$

where

$$\Lambda_0 = \frac{2}{X} \int_{-X/2}^{X/2} \lambda(x) dx \tag{A.20}$$

$$= \frac{2}{X} \left(\lambda_2 X_2 + \lambda_1 X_1\right) \tag{A.21}$$

$$\Lambda_q = \frac{2}{X} \int_{-X/2}^{X/2} \lambda(x) \cos(n2\pi x/X) dx \tag{A.22}$$

$$= \frac{2}{X} \left(\lambda_2 \int_{-X/2}^{-X_1/2} \cos(n2\pi x/X) dx + \lambda_1 \int_{-X_1/2}^{X_1/2} \cos(n2\pi x/X) dx \right. \tag{A.23}$$

$$\left. + \lambda_2 \int_{X_1/2}^{X/2} \cos(n2\pi x/X) dx \right) \tag{A.24}$$

$$= \frac{2}{q\pi} \left(\lambda_2 \left(\sin(q\omega_0 X/2) - \sin(q\omega_0 X_1/2)\right) + \lambda_1 \sin(q\omega_0 X_1/2)\right) \tag{A.25}$$

$$= \frac{2}{q\pi} \left(\lambda_2 \left(\sin(q\pi) - \sin(q\pi X_1/X)\right) + \lambda_1 \sin(q\pi X_1/X)\right) \tag{A.26}$$

A.7 Jacobi-Anger expansion

One of the forms of Jacobi-Anger expansion is

$$e^{iz\cos(\Phi)} = \sum_{n=-\infty}^{\infty} i^n J_n(z) e^{in\Phi}. \tag{A.27}$$

A.8 Bessel Functions

A special relation of Bessel function is that

$$J_n(n\operatorname{sech}\alpha) \sim \frac{e^{n(\tanh\alpha-\alpha)}}{\sqrt{2\pi n \tanh\alpha}} \tag{A.28}$$

for large n [20]. As a matter of fact, for all positive α, we always have $\tanh\alpha - \alpha < 0$.

Using this relation and defining $\operatorname{sech}\alpha = A\cos 2\theta_m$, which renders

$$\alpha = 2n\pi i + \ln\left(\frac{1 \pm \sqrt{-A^2\cos^2 2\theta_m + 1}}{A\cos 2\theta_m}\right), \qquad n \in \text{Integers}, \tag{A.29}$$

where the Mathematica code to solve it is shown below,

```
In[1]:= Solve[Exp[z] + Exp[-z]
== 2/(A Cos[2 Subscript[\[Theta], m]]), z] // FullSimplify
```

we find out an more human readable analytical expression for the width

$$\Gamma = \left|2\hat{k}\tan 2\theta_m \frac{e^{n(\tanh\alpha-\alpha)}}{n_0\sqrt{2\pi n_0 \tanh\alpha}}\right| \tag{A.30}$$

where α is solved out in A.29. For small α, we have expansions for exponential functions and hyperbolic functions $\tanh\alpha \sim \alpha - \frac{\alpha^3}{3}$,

$$\Gamma \asymp 2\tan 2\theta_m \frac{e^{n\alpha^3/3}}{\sqrt{2\pi\alpha}n_0^{3/2}}. \tag{A.31}$$

However, it doesn't really help that much since n is large and no expansion could be done except for significantly small α.

A.9 Conversions in Neutrino Physics

Using natural units, length $=$ time $= 1/$energy, we could rescale almost all quantities in neutrino oscillations using energy, or whatever characteristic scale we have.

We use two flavor vacuum oscillations between the two masses m_1 and m_2 as an example. The characteristic energy scale is the oscillation frequency $\omega_{v,21}$. The equation of motion

$$i\frac{d}{dx}\Psi = \frac{\omega_v}{2}(-\cos 2\theta_v \boldsymbol{\sigma_3} + \sin 2\theta_v \boldsymbol{\sigma_1})\Psi, \tag{A.32}$$

can be rescaled using the characteristic energy scale $\omega_{v,21}$

$$i\frac{d}{d\hat{x}}\Psi = \frac{1}{2}(-\cos 2\theta_v \boldsymbol{\sigma_3} + \sin 2\theta_v \boldsymbol{\sigma_1})\Psi, \tag{A.33}$$

where $\hat{x} = \omega_{v,21}x$. It is convenient for numerical calculations to convert quantities into dimensionless ones.

However, we usually discuss oscillation length in SI units for a grip of the picture. To convert from natural units to SI units, we write down the conversion here. The oscillation angular frequency is given by

$$\begin{aligned}
\omega_{v,21} &= \frac{\delta m^2}{2E}\\
&= \left(\frac{7.5 \times 10^{-5}\text{eV}^2}{2 \times 1\text{MeV}}\right)\left(\frac{\delta m^2}{7.5 \times 10^{-5}\text{eV}^2}\right)\frac{1\text{MeV}}{E}\\
&= 3.75 \times 10^{-11}\text{eV}\left(\frac{\delta m^2}{7.5 \times 10^{-5}\text{eV}^2}\right)\left(\frac{1\text{MeV}}{E}\right).
\end{aligned} \tag{A.34}$$

On the other hand, electro-volt is related to length through the useful formula

$$197\text{MeV} \cdot \text{fm} = \hbar c = 1. \tag{A.35}$$

Thus we have the oscillation angular frequency written as

$$\begin{aligned}
\omega_{v,21} &= 3.75 \times 10^{-11}\text{eV}\frac{\delta m^2}{7.5 \times 10^{-5}\text{eV}^2}\frac{1\text{MeV}}{E}\\
&= 3.75 \times 10^{-17}\text{MeV}\frac{\delta m^2}{7.5 \times 10^{-5}\text{eV}^2}\frac{1\text{MeV}}{E}\\
&= 1.90 \times 10^{-4}\text{m}^{-1}\frac{\delta m^2}{7.5 \times 10^{-5}\text{eV}^2}\frac{1\text{MeV}}{E}.
\end{aligned} \tag{A.36}$$

Similarly for $\delta m_{32} = 2.4 \times 10^{-3}\text{eV}^2$ the frequency is

$$\omega_{v,32} = \frac{\delta m_{32}^2}{2E} = 6.3 \times 10^{-3}\text{m}^{-1}\frac{\delta m_{32}^2}{2.5 \times 10^{-3}\text{eV}^2}\frac{1MeV}{E}. \tag{A.37}$$

With the results for angular frequencies, the rescaled length $\hat{x}$ is restored using

$$x = \frac{\hat{x}}{\omega_v} = \frac{\hat{x}}{1.90 \times 10^{-4} \mathrm{m}^{-1} \frac{\delta m^2}{7.5 \times 10^{-5} \mathrm{eV}^2} \frac{1\mathrm{MeV}}{E}} \tag{A.38}$$

$$= \frac{\hat{x}}{0.190} \mathrm{km} \frac{7.5 \times 10^{-5} \mathrm{eV}^2}{\delta m^2} \frac{E}{1\mathrm{MeV}}. \tag{A.39}$$

Another important example is the 2 flavor neutrino oscillations in constant matter background potential $\lambda_c = \sqrt{2} G_\mathrm{F} n_e$. The characteristic energy scale is ω_m which is calculated using

$$\omega_m = \omega_v \sqrt{\frac{\lambda_c}{\omega_v}^2 + 1 - 2\frac{\lambda_c}{\omega_v} \cos 2\theta_v}. \tag{A.40}$$

Meanwhile, the effective mixing angle θ_m is determined by

$$\tan 2\theta_m = \frac{\sin 2\theta_v}{\cos 2\theta_v - \frac{\lambda}{\omega_v}}. \tag{A.41}$$

Similar to vacuum equation of motion, we rescale the equation of motion in constant background using ω_m

$$i\frac{d}{d\hat{x}}\Psi = \frac{1}{2}\left(-\cos 2\theta_m \boldsymbol{\sigma_3} + \sin 2\theta_m \boldsymbol{\sigma_1}\right)\Psi, \tag{A.42}$$

we find out the scaled distance

$$\hat{x} = \omega_m x. \tag{A.43}$$

To reverse the process and find out the actual SI unit distance after the numerical calculation, we use

$$x = \frac{\hat{x}}{\omega_m}. \tag{A.44}$$

The procedure will be the following.

- Calculate ω_v using Eq. A.36.

- Calculate $\hat{\lambda}_c = \frac{\lambda_c}{\omega_v}$.

- Calculate ω_m using Eq. A.40.

- Find out the actual distance using Eq. A.44.

Appendix B

MSW Effect Revisited

B.1 Flavor Basis

In terms of formalism, vacuum oscillations is already a Rabi oscillation at resonance with oscillation width $\omega_v \sin 2\theta_v$. As derived, neutrino oscillations in matter are determined by Hamiltonian in flavor basis

$$H^{(f)} = \left(-\frac{1}{2}\omega_v \cos 2\theta_v + \frac{1}{2}\lambda(x) \right) \sigma_3 + \frac{1}{2}\omega_v \sin 2\theta_v \sigma_1, \tag{B.1}$$

with the Schröding equation

$$i\partial_x \Psi^{(f)} = H^{(f)}\Psi^{(f)}. \tag{B.2}$$

To make connections to Rabi oscillations, we would like to remove the changing σ_3 terms, using a transformation

$$U = \begin{pmatrix} e^{-i\eta(x)} & 0 \\ 0 & e^{i\eta(x)} \end{pmatrix}, \tag{B.3}$$

which transform the flavor basis to another basis

$$\begin{pmatrix} \psi_e \\ \psi_x \end{pmatrix} = \begin{pmatrix} e^{-i\eta(x)} & 0 \\ 0 & e^{i\eta(x)} \end{pmatrix} \begin{pmatrix} \psi_a \\ \psi_b \end{pmatrix}. \tag{B.4}$$

The Schrodinger equation can be written into this new basis

$$i\partial_x(T\Psi^{(r)}) = H^{(f)}T\Psi^{(r)}, \tag{B.5}$$

which is simplified to

$$i\partial_x \Psi^{(r)} = H^{(r)} \Psi^{(r)}, \tag{B.6}$$

where

$$H^{(r)} = -\frac{1}{2}\omega_v \cos 2\theta_v \sigma_3 + \frac{1}{2}\omega_v \sin 2\theta_v \begin{pmatrix} 0 & e^{2i\eta(x)} \\ e^{-2i\eta(x)} & 0 \end{pmatrix}, \tag{B.7}$$

in which we remove the varying component of σ_3 elements using

$$\frac{d}{dx}\eta(x) = \frac{\lambda(x)}{2}. \tag{B.8}$$

The final Hamiltonian would have some form

$$H^{(r)} = -\frac{1}{2}\omega_v \cos 2\theta_v \sigma_3 + \frac{1}{2}\omega_v \sin 2\theta_v \begin{pmatrix} 0 & e^{i\int_0^x \lambda(\tau)d\tau + 2i\eta(0)} \\ e^{-i\int_0^x \lambda(\tau)d\tau - 2i\eta(0)} & 0 \end{pmatrix}, \tag{B.9}$$

where $\eta(0)$ is chosen to counter the constant terms from the integral.

For arbitrary matter profile, we could first apply Fourier expand the profile into trig function then use Jacobi-Anger expansion so that the system becomes a lot of Rabi oscillations. Any transformations or expansions that decompose $\exp\left(i\int_0^x \lambda(\tau)d\tau\right)$ into many summations of $\exp(iax + b)$ would be enough for an Rabi oscillation interpretation. As for constant matter profile, $\lambda(x) = \lambda_0$, we have

$$\eta(x) = \frac{1}{2}\lambda_0 x. \tag{B.10}$$

The Hamiltonian becomes

$$H^{(r)} = -\frac{1}{2}\omega_v \cos 2\theta_v \sigma_3 + \frac{1}{2}\omega_v \sin 2\theta_v \begin{pmatrix} 0 & e^{i\lambda_0 x} \\ e^{-i\lambda_0 x} & 0 \end{pmatrix}, \tag{B.11}$$

which is exactly a Rabi oscillation. The resonance condition is

$$\lambda_0 = \omega_v \cos 2\theta_v. \tag{B.12}$$

B.2   Instantaneous Matter Basis

Neutrino oscillations can be calculated in instantaneous matter basis, where the Schrödinger equation is transformed to instantaneous matter basis by applying a

rotation U,

$$i\partial_x \left(U\Psi^{(m)} \right) = H^{(f)} U\Psi^{(m)}, \tag{B.13}$$

where

$$U = \begin{pmatrix} \cos\theta_m & \sin\theta_m \\ -\sin\theta_m & \cos\theta_m \end{pmatrix}. \tag{B.14}$$

With some simple algebra, we can write the system into

$$i\partial_x \Psi^{(m)} = H^{(m)}\Psi^{(m)}, \tag{B.15}$$

where

$$H^{(m)} = U^\dagger H^{(f)} U - iU^\dagger \partial_x U. \tag{B.16}$$

By setting the off-diagonal elements of the first term $U^\dagger H^{(f)} U$ to zero, we can derive the relation

$$\tan 2\theta_m = \frac{\sin 2\theta_v}{\cos 2\theta_v - \lambda/\omega_v}. \tag{B.17}$$

Furthermore, we derive the term

$$iU^\dagger \partial_x U = -\dot{\theta}_m \sigma_2. \tag{B.18}$$

We can calculate $\dot{\theta}_m$ by taking the derivative of $\tan 2\theta_m$,

$$\frac{d}{dx}\tan 2\theta_m = \frac{2}{\cos^2 2\theta_m}\dot{\theta}_m, \tag{B.19}$$

so that

$$\dot{\theta}_m = \frac{1}{2}\cos^2(2\theta_m)\frac{d}{dx}\tan 2\theta_m \tag{B.20}$$

$$= \frac{1}{2}\frac{(\cos 2\theta_v - \lambda/\omega_v)^2}{(\lambda/\omega_v)^2 + 1 - 2\lambda\cos 2\theta_v/\omega_v}\frac{d}{dx}\frac{\sin 2\theta_v}{\cos 2\theta_v - \lambda/\omega_v} \tag{B.21}$$

$$= \frac{1}{2}\frac{(\cos 2\theta_v - \lambda/\omega_v)^2}{(\lambda/\omega_v)^2 + 1 - 2\lambda\cos 2\theta_v/\omega_v}\frac{\sin 2\theta_v}{(\cos 2\theta_v - \lambda/\omega_v)^2}\frac{1}{\omega)v}\frac{d}{dx}\lambda(x) \tag{B.22}$$

$$= \frac{1}{2}\sin 2\theta_m \frac{1}{\omega_m}\frac{d}{dx}\lambda(x). \tag{B.23}$$

B.3 Bipolar Model

The nature of this section is to provide the linear stability analysis of bipolar model. Bipolar model is a model of neutrino oscillations with the presence of neutrino and

antineutrinos. It is also called bimodal oscillations [10], which means two frequencies in the context. An example of such instability happens in a system composed of equal amounts of neutrinos and antineutrinos.

Neutrino oscillations has a small amplitude inside a SN core (suppressed by matter effects) [5], which basically pins down the flavour transformation. As the neutrinos reaches a further distance, matter effect could drop out. Neutrino self-interaction becomes more important. S. Samuel considers a system of neutrinos and antineutrinos with only vacuum and neutrino self-interactions [10]. The neutrinos and antineutrino forms a bipolar vector in flavor isospin space. The flavor isospin of neutrinos and that of antineutrinos are coupled.

The equation of motion is

$$i\partial_t \rho = \left[-\frac{\omega_v}{2} \cos 2\theta \sigma_3 + \frac{\omega_v}{2} \sin 2\theta \sigma_1 - \mu \alpha \bar{\rho}, \rho \right]$$
$$i\partial_t \bar{\rho} = \left[\frac{\omega_v}{2} \cos 2\theta \sigma_3 - \frac{\omega_v}{2} \sin 2\theta \sigma_1 + \mu \rho, \bar{\rho} \right].$$

For the purpose of linear stability analysis, we assume that

$$\rho = \frac{1}{2} \begin{pmatrix} 1 & \epsilon \\ \epsilon^* & -1 \end{pmatrix}$$

$$\bar{\rho} = \frac{1}{2} \begin{pmatrix} 1 & \bar{\epsilon} \\ \bar{\epsilon}^* & -1 \end{pmatrix}.$$

Plug them into equation of motion and set $\theta = 0$, we have the linearized ones,

$$i\partial_t \begin{pmatrix} \epsilon \\ \bar{\epsilon} \end{pmatrix} = \frac{1}{2} \begin{pmatrix} -\alpha\mu - \omega_v & \alpha\mu \\ -\mu & \mu + \omega_v \end{pmatrix} \begin{pmatrix} \epsilon \\ \bar{\epsilon} \end{pmatrix}.$$

To have real eigenvalues, we require

$$(-1 + \alpha)^2 \mu^2 + 4(1 + \alpha)\mu\omega_v + 4\omega_v^2 < 0,$$

which is reduced to

$$\frac{-2\omega_v(1 + \alpha) - 4\sqrt{\alpha}|\omega_v|}{(1 - \alpha)^2} < \mu < \frac{-2\omega_v(1 + \alpha) + 4\sqrt{\alpha}|\omega_v|}{(1 - \alpha)^2}.$$

It is simplified to

$$\sqrt{-2\omega_v}(1 - \sqrt{\alpha})^2 < \mu < \sqrt{-2\omega_v}(1 + \sqrt{\alpha})^2,$$

assuming normal hierarchy, i.e., $\omega_v > 0$. We immediately notice that this can not happen.

For inverted hierarchy, we have $\omega_v < 0$, so that

$$\sqrt{2|\omega_v|}(1 + \sqrt{\alpha})^2 < \mu < \sqrt{2|\omega_v|}(1 - \sqrt{\alpha})^2,$$

Within this region, neutrinos experience exponential growth.

For completeness, we also write down the formalism in flavor isospin picture.

$$i\partial_t \mathbf{s} = \mathbf{s} \times (\eta \mathbf{H}_v + \alpha\mu\bar{\mathbf{s}}) \tag{B.24}$$

$$i\partial_t \bar{\mathbf{s}} = \bar{\mathbf{s}} \times (\eta \mathbf{H}_v + \mu\mathbf{s}), \tag{B.25}$$

where η is the hierarchy, and α is the ratio of neutrino number density and antineutrino number density.

Bibliography

[1] C. L. Cowan, F. Reines, F. B. Harrison, H. W. Kruse, and A. D. McGuire, "Detection of the Free Neutrino: a Confirmation.", Science (New York, N.Y.) **124**, 103–4 (1956).

[2] B. Pontecorvo, "Neutrino experiments and the problem of conservation of leptonic charge", Sov. Phys. JETP **26**, 984–988 (1968).

[3] J. Bahcall, "The solar neutrino problem", Nuclear Instruments and Methods **110**, 381–384 (1973).

[4] E. G. Flowers and P. G. Sutherland, "Neutrino-neutrino scattering and supernovae", The Astrophysical Journal **208**, L19 (1976).

[5] L. Wolfenstein, "Neutrino oscillations in matter", Physical Review D **17**, 2369–2374 (1978).

[6] J. N. Bahcall, A. Dar, and T. Piran, "Neutrinos from the recent LMC supernova", Nature **326**, 135–136 (1987).

[7] P. Krastev and A. Smirnov, "Parametric effects in neutrino oscillations", Physics Letters B **226**, 341–346 (1989).

[8] G. Sigl and G. Raffelt, "General kinetic description of relativistic mixed neutrinos", Nuclear Physics B **406**, 423–451 (1993).

[9] F. N. Loreti and A. B. Balantekin, "Neutrino oscillations in noisy media", Physical Review D **50**, 4762–4770 (1994).

[10] S. Samuel, "Bimodal coherence in dense self-interacting neutrino gases", Physical Review D **53**, 5382–5393 (1996).

[11]E. Akhmedov, "Parametric resonance of neutrino oscillations and passage of solar and atmospheric neutrinos through the earth", Nuclear Physics B **538**, 25–51 (1999).

[12]E. K. Akhmedov, "Parametric resonance in neutrino oscillations in matter", Pramana **54**, 47–63 (2000).

[13]M. F. Altmann, R. L. Mößbauer, and L. J. N. Oberauer, "Solar neutrinos", Reports on Progress in Physics **64**, 97–146 (2001).

[14]S. Pastor, G. Raffelt, and D. V. Semikoz, "Physics of synchronized neutrino oscillations caused by self-interactions", Physical Review D **65**, 053011 (2002).

[15]H. Duan, G. M. Fuller, J. Carlson, and Y. Z. Qian, "Simulation of coherent nonlinear neutrino flavor transformation in the supernova environment: Correlated neutrino trajectories", Physical Review D - Particles, Fields, Gravitation and Cosmology **74**, 1–22 (2006).

[16]H. Duan, G. M. Fuller, and Y.-Z. Qian, "Analysis of collective neutrino flavor transformation in supernovae", Physical Review D **74**, 123004 (2006).

[17]A. Friedland and A. Gruzinov, "Neutrino signatures of supernova turbulence", July 2006.

[18]S. Hannestad, G. G. Raffelt, G. Sigl, and Y. Y. Y. Wong, "Self-induced conversion in dense neutrino gases: Pendulum in flavor space", Physical Review D - Particles, Fields, Gravitation and Cosmology **74**, 1–21 (2006).

[19]G. G. Raffelt, "Self-induced parametric resonance in collective neutrino oscillations", Physical Review D - Particles, Fields, Gravitation and Cosmology **78**, 1–9 (2008).

[20]I. Ploumistakis, S. D. Moustaizis, and I. Tsohantjis, "Towards laser based improved experimental schemes for multiphoton e+e-pair production from vacuum", Physics Letters, Section A: General, Atomic and Solid State Physics **373**, 2897–2900 (2009).

[21]H. Duan, G. M. Fuller, and Y.-Z. Qian, "Collective Neutrino Oscillations", Annual Review of Nuclear and Particle Science **60**, 569–594 (2010).

[22] J. Kneller and C. Volpe, "Turbulence effects on supernova neutrinos", Physical Review D **82**, 123004 (2010).

[23] E. Adelberger and a. García, "Solar fusion cross sections. II. The pp chain and CNO cycles", Reviews of Modern … **83** (2011).

[24] J. F. Cherry, J. Carlson, A. Friedland, G. M. Fuller, and A. Vlasenko, "Neutrino scattering and flavor transformation in supernovae", Physical Review Letters **108**, 1–5 (2012).

[25] O. Pejcha and T. A. Thompson, "THE PHYSICS OF THE NEUTRINO MECHANISM OF CORE-COLLAPSE SUPERNOVAE", The Astrophysical Journal **746**, 106 (2012).

[26] S. Sarikas, I. Tamborra, G. Raffelt, L. Hüdepohl, and H. T. Janka, "Supernova neutrino halo and the suppression of self-induced flavor conversion", Physical Review D - Particles, Fields, Gravitation and Cosmology **85**, 1–5 (2012).

[27] J. P. Kneller, G. C. McLaughlin, and K. M. Patton, "Stimulated neutrino transformation with sinusoidal density profiles", Journal of Physics G: Nuclear and Particle Physics **40**, 055002 (2013).

[28] K. M. Patton, J. P. Kneller, and G. C. McLaughlin, "Stimulated neutrino transformation through turbulence", Physical Review D **89**, 073022 (2014).

[29] S. M. Couch and C. D. Ott, "The Role of Turbulence in Neutrino-driven Core-collapse Supernova Explosions", The Astrophysical Journal **799**, 5 (2015).

[30] B. Muller and H.-. T. Janka, "Non-radial instabilities and progenitor asphericities in core-collapse supernovae", Monthly Notices of the Royal Astronomical Society **448**, 2141–2174 (2015).

[31] K. M. Patton, J. P. Kneller, and G. C. McLaughlin, "Stimulated neutrino transformation through turbulence on a changing density profile and application to supernovae", Phys. Rev. **D91**, 025001 (2015).

[32] S. Chakraborty, R. S. Hansen, I. Izaguirre, and G. Raffelt, "Self-induced neutrino flavor conversion without flavor mixing", Journal of Cosmology and Astroparticle Physics **2016**, 042–042 (2016).

[33]H.-T. Janka, T. Melson, and A. Summa, "Physics of Core-Collapse Supernovae in Three Dimensions: A Sneak Preview", Annual Review of Nuclear and Particle Science **66**, 341–375 (2016).

[34]C. Patrignani et al., "Review of Particle Physics", Chin. Phys. **C40**, 100001 (2016).

[35]R. F. Sawyer, "Neutrino Cloud Instabilities Just above the Neutrino Sphere of a Supernova", Physical Review Letters **116**, 1–5 (2016).

[36]F. Capozzi, B. Dasgupta, E. Lisi, A. Marrone, and A. Mirizzi, "Fast flavor conversions of supernova neutrinos: Classifying instabilities via dispersion relations", Physical Review D **96**, 1–20 (2017).

[37]I. Izaguirre, G. Raffelt, and I. Tamborra, "Fast Pairwise Conversion of Supernova Neutrinos: A Dispersion Relation Approach", Physical Review Letters **118**, 021101 (2017).

[38]H.-T. Janka, *Neutrino emission from supernovae*, edited by A. W. Alsabti and P. Murdin (Springer International Publishing, Cham, 2017), pp. 1575–1604.

[39]E. Kemp, "The Deep Underground Neutrino Experiment: The precision era of neutrino physics", Astronomische Nachrichten **338**, 993–999 (2017).